UASLP
Universidad Autónoma de San Luis Potosí

FACULTAD DE CIENCIAS UASLP

Propuesta de inhibidores químicos que compiten con la unión de las subunidades de la RNA polimerasa II a las GTPasas esenciales Npa3 y Gpn1

Tesis que para obtener el grado de Doctor en Ciencias Interdisciplinarias presenta:

MCI Julio Alberto Muñiz Luna

Línea de Investigación:

Bioquímica y Biología Celular

Codirectores de Tesis:

Dr. Roberto Sánchez Olea

Dra. Mónica Raquel Calera Medina

San Luis Potosí, S.L.P., a 8 de diciembre del 2025

POSGRADO EN CIENCIAS INTERDISCIPLINARIAS

UASLP Instituto de Física

JURADO EVALUADOR

Secretario: Dr. Pedro Ezequiel Ramírez González

Presidente: Dr. Juan Rodrigo Vélez Cordero

Suplente: Dr. José Guadalupe Sampedro Pérez

Sinodal externo: Dr. José Ángel Santiago Terrones

Vocal: Dra. Mónica Raquel Calera Medina

Vocal: Dr. Roberto Sánchez Olea

CRÉDITOS INSTITUCIONALES

La presente tesis fue realizada en los Laboratorios de Biología Celular y Biología Molecular del Instituto de Física de la Universidad Autónoma de San Luis Potosí bajo la dirección del Dr. Roberto Sánchez Olea y de la Dra. Mónica Raquel Calera Medina. Se agradece el apoyo del Consejo Nacional de Humanidades, Ciencias y Tecnologías (Conahcyt, ahora SECIHTI: Secretaría de Ciencia, Humanidades, Tecnologías e Innovación) por otorgar la beca no. 723271 al MCI Julio Alberto Muñiz Luna. Para la realización de este trabajo se contó con la aportación del Proyecto de Ciencia Básica Conahcyt (ahora SECIHTI) no. A1-S-21070 (RSO) y con el apoyo del Laboratorio Nacional de Supercómputo proyecto no. 202201035N (MRC).

RESUMEN

Las proteínas Gpn1, Gpn2 y Gpn3 son miembros de la familia de GTPasas GPN; Npa3 en la levadura *Saccharomyces cerevisiae* es el ortólogo de Gpn1 humana. Estas proteínas desempeñan un papel crucial en el ensamble y en la acumulación nuclear de la RNA polimerasa II (RNAPII), funcionando como chaperonas moleculares. Las estructuras cristalográficas de Npa3 revelan conformaciones abiertas y cerradas, dependiendo del nucleótido de guanina unido (GMPPCP, un análogo no hidrolizable del GTP, o GDP, respectivamente). La conformación abierta de Npa3 posee una cavidad hidrofóbica que es sugerida como esencial para el reconocimiento y la unión de subunidades de la RNAPII durante su biogénesis; sin embargo, aún no se dispone de datos estructurales sobre estos complejos. En este trabajo, se generaron modelos *in silico* de las interacciones entre la estructura cristalográfica de Npa3 monomérica en su conformación abierta y péptidos de la RNAPII de levadura que se han demostrado experimentalmente interactúan con Npa3, generados mediante acoplamiento computacional flexible. Con la finalidad de identificar inhibidores de estas interacciones, potencialmente útiles para comprender las funciones moleculares y celulares de estas proteínas, se realizaron experimentos de acoplamiento molecular utilizando una biblioteca diseñada de compuestos aprobados por la FDA, tanto en la estructura experimental de Npa3 como en un modelo por homología de Gpn1 humana. Se identificaron, tras una optimización por acoplamiento flexible, como potenciales inhibidores competitivos el fármaco atovacuona para Npa3 y Gpn1 (energías de afinidad de −14,4 y −13,5 kcal/mol, respectivamente) y tibolona para Npa3 (−13,6 kcal/mol). Además, nuestros modelos de acoplamiento sugieren residuos clave en Npa3, como F143 y W179, que pueden ser fundamentales para el reconocimiento tanto de las subunidades de la RNAPII como de los fármacos. En el futuro, estudios bioquímicos y de mutagénesis sitio dirigida podrán aportar evidencia funcional sobre su efecto en la biogénesis de la RNAPII.

ABSTRACT

The Gpn1, Gpn2, and Gpn3 proteins are members of the GPN-loop GTPase family; budding yeast Npa3 is an orthologue of the human Gpn1. These proteins play a crucial role in the assembly and nuclear localization of RNA polymerase II (RNAPII), functioning as molecular chaperones. The crystallographic structures of Npa3 reveal open and closed conformations, which are dependent on the bound guanine nucleotide (GMPPCP or GDP, respectively). The open conformation of Npa3 exhibits a hydrophobic pocket proposed to be essential for the recognition and binding of specific peptides of RNAPII, contributing to its biogenesis; however, structural data on these complexes remain unavailable. In this work, we present in silico models of the interactions between the crystallographic structure of monomeric Npa3 in its open conformation and yeast RNA polymerase II peptides, generated through flexible computational docking. To identify inhibitors of these interactions, potentially useful in understanding the molecular and cellular functions of these proteins, we performed molecular docking experiments using a designed library of FDA-approved compounds on both the Npa3 structure and a homology model of human Gpn1. Our analysis identified potential inhibitors, including atovaquone for both Npa3 and Gpn1 (docking scores: −14.4 and −13.5 kcal/mol, respectively) and tibolone for Npa3 (−13.6 kcal/mol), following flexible docking optimization. Additionally, our docking models suggest key residues in Npa3 such as F143 and W179, which may be critical for recognizing RNAPII subunits and druglike molecules. These findings can be further explored through biochemical and mutagenesis studies to assess their roles in RNAPII.

GRAPHICAL ABSTRACT

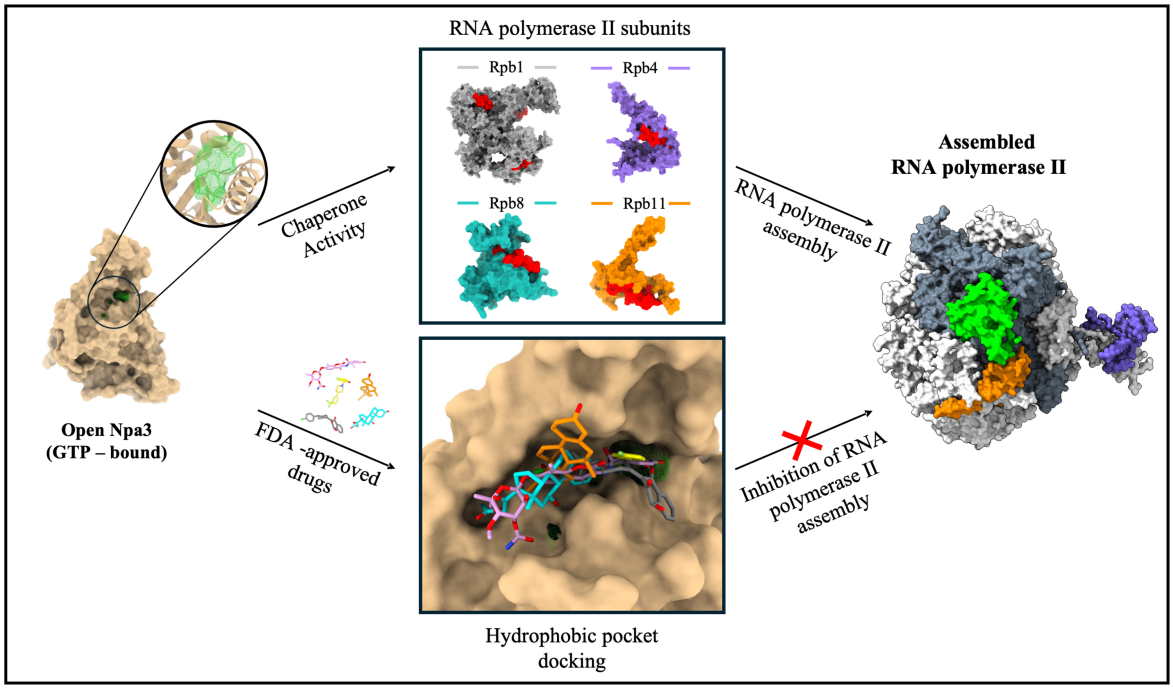

AGRADECIMIENTOS Y DEDICATORIA

Dedico con inmenso amor el presente trabajo, a mis hijos, Valentina y Leonardo, y a Diana, mi esposa**.** Son todo en mi vida y representan una fuente inagotable de motivación e inspiración. Con el corazón lleno de gratitud, deseo resaltar el invaluable apoyo y participación de Diana, quien caminó junto a mí en cada etapa de este proceso, con su inmenso amor, consejo, orientación e inspiración diaria que me ayudan a ser una mejor versión de mí cada día. Su fortaleza, que siempre he admirado, fue para mí un sostén de valor incalculable. A Valentina, noble y cariñosa, y a Leonardo, siempre alegre y lleno de luz; ambos, fueron el sentido más profundo de este trabajo.

A mis padres, tuve la fortuna de crecer bajo el cuidado de las personas más bondadosas y de corazón más noble que conozco. No existe vida suficiente para retribuir todo lo que han hecho por mí. A mi mamá, mujer de ciencia que sembró desde mi infancia la semilla de la curiosidad por aprender y apreciar los detalles del mundo, aun en sus formas más sencillas. Agradezco, además, su participación directa en mi formación académica como mi maestra.

A mi papá, por ser el mayor ejemplo de serenidad, por educarme a través de sus acciones y por velar siempre para que pudiera formarme en un entorno de paz y tranquilidad. Le expreso mi profundo agradecimiento por haber priorizado siempre y de forma incondicional mi educación.

Agradezco a mis directores de tesis, a la Dra. Mónica Raquel Calera Medina y al Dr. Roberto Sánchez Olea, por su guía generosa, por abrirme con confianza las puertas de su laboratorio y por el trato siempre cordial y respetuoso que me brindaron a lo largo de estos años. A la Dra. Nina Pastor Colón, por sus aportaciones fundamentales al desarrollo de este trabajo y por la guía experimental que siempre me ofreció con generosidad.

A la Dra. Gema Cristóbal Mondragón y al Dr. Ángel Santiago, por su impecable trabajo y su valiosa contribución técnica e intelectual. Asimismo, valoro profundamente la amistad y el apoyo incondicional que me brindaron desde el inicio de este proyecto y en momentos cruciales del desarrollo de esta tesis.

Finalmente, a mis compañeros y amigos de laboratorio, en los inicios de este proyecto, Yolanda, Gris, Alda, Grecia, Andrea, Karla, Tania, Fernando y Martín; y en tiempos recientes, Cristhian, Dulce, Boris, Alberto, Ximena, Liz, Regina, Sofía, Mónica, Emmanuel, Bernardo y Estefanía. Todos ellos me acompañaron cotidianamente y estuvieron siempre atentos a mi bienestar y al progreso del proyecto.

ÍNDICE

1. INTRODUCCIÓN.

1.1 GTPasas

Las GTPasas son una superfamilia de enzimas que poseen una alta afinidad por los nucleótidos de guanina y tienen la capacidad para hidrolizar GTP a GDP (Pai et al., 1989; Bourne HR et al., 1991; Rojas et al., 2012). Estas proteínas actúan como *switches* o interruptores moleculares alternando entre un estado activo, donde se encuentra unido el GTP, y un estado inactivo, unido al GDP (Figura 1) (Hall, 1990; Takai et al., 2001; Vetter & Wittinghofer, 2001). Participan en una gran variedad de funciones celulares, incluyendo la transducción de señales, síntesis de proteínas, migración celular, tráfico vesicular y la reorganización del citoesqueleto (Takai et al., 2001; Leipe et al., 2002; Wennerberg et al., 2005; Charest & Firtel, 2007; Yalovsky et al., 2008). Estructuralmente, comparten un dominio que es esencial para la unión de los nucleótidos de guanina GTP y GDP, e hidrólisis del GTP; consta de 170 residuos y poseen los motivos característicos nombrados G1 a G5 (Bourne HR et al., 1991; Sprang, 1997; Paduch et al., 2001; Reiner, 2018). Los primeros estudios reportados sobre proteínas con actividad de GTPasa surgieron entre las décadas de 1950 y 1960, siendo el trabajo de J. Gordon en 1969, uno de los primeros en describir el proceso de hidrólisis enzimática del guanosín trifosfato (Gordon, 1969). Las investigaciones realizadas en estas décadas no empleaban el término GTPasa, sin embargo, demostraron la existencia de proteínas con actividad de GTP hidrolasa asociadas a funciones celulares específicas. En la década de 1970, Martín Rodbell publicó varios artículos sobre la regulación de la adenilato ciclasa o adenilil ciclasa por GTP y su relación con receptores hormonales (Rodbell et al., 1971; Birnbaumer et al., 1971; Londos et al., 1974), antes de que se definiera formalmente el concepto de “proteínas G”. Posteriormente, a inicios de 1980, los trabajos de Channing J. Der y colaboradores llevaron a la identificación de los oncogenes humanos *H-Ras* y *K-Ras* en líneas celulares de carcinoma de vejiga y pulmón, homólogos a los oncogenes virales *v-Ha-ras* y *v-Ki-ras* de retrovirus de ratas (Der et al., 1982). En ese mismo año, se publicó un estudio en la revista *Nature* donde identificaron al oncogén humano de vejiga (*T24/H-ras*) como homólogo del oncogén viral *v-Ha-ras*,

estableciendo por primera vez la existencia de un protooncogén *ras* humano (Santos et al., 1982). Estos hallazgos contribuyeron al establecimiento del concepto de las GTPasas pequeñas como interruptores moleculares en la regulación del crecimiento celular.

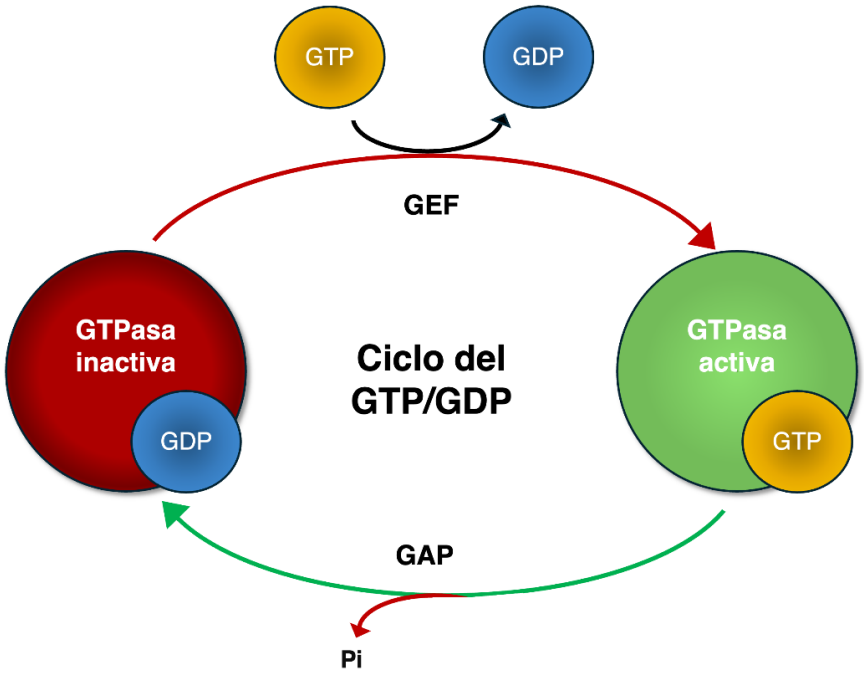

Figura 1. Ciclo de las GTPasas. La unión de los nucleótidos de guanina GTP y GDP determina la estructura y función de las GTPasas. Se consideran activas cuando están unidas al GTP, en dicho estado son capaces de interactuar con su efector para generar diversos efectos biológicos. La intervención de proteínas accesorias como los factores activadores de GTPasas (GAPs) favorecen la hidrólisis del GTP, que mediante la hidrólisis del fosfato gama es convertido en GDP, entrando así en un estado inactivo. Por otro lado, los factores intercambiadores de nucleótidos de guanina (GEFs), facilitan el desprendimiento del GDP, y como consecuencia la unión de una nueva molécula de GTP, dando inicio nuevamente al ciclo de activación e inactivación de las GTPasas.

En 1982, Walker, J. E. y colaboradores identificaron por primera vez el motivo conservado GXXXXGKT, conocido posteriormente "*Walker A motif*" o *P-loop* (motivo

de unión al fosfato), mediante el estudio de los sitios de unión al ATP de las cinasas y otras enzimas que unen ATP (Walker et al., 1982). Este descubrimiento estableció que proteínas escasamente emparentadas comparten un pliegue común que participa en la unión de nucleótidos. Las implicaciones de este descubrimiento contribuyeron a la comprensión estructural de las proteínas de unión a nucleótidos. Estudios comparativos posteriores de las secuencias de proteínas Ras y otras GTPasas, demostraron que comparten el motivo *P-loop*, conocido en estas enzimas como motivo G1 (Valencia et al., 1991), además de otros cuatro motivos estructurales conservados y característicos (G2-G5) del dominio G. Durante los años noventa, el estudio de las GTPasas trascendió desde la identificación de proteínas Ras a una comprensión sobre sus mecanismos de regulación, las interacciones que establecen con efectores, y cómo se diversifican funcionalmente en rutas celulares específicas. En esta época, se consolidó la clasificación de las GTPasas pequeñas en cinco familias principales, cada una con funciones celulares específicas: Ras, Rho, Rab, Arf/Sar y Ran. Este grupo de enzimas comparten un mecanismo molecular en común de encendido y apagado, dependiente de la unión de GTP y GDP, respectivamente. Estudios cristalográficos revelaron que las GTPasas presentan cambios conformacionales en dos regiones críticas nombradas como "*switch 1*" y "*switch 2*" (Milburn et al., 1990). También, fueron descritos los procesos regulatorios de estas enzimas mediante las proteínas accesorias GEFs (*guanine nucleotide exchange factors*) y GAPs (*GTPase-activating proteins*), por sus siglas en inglés (Bourne et al., 1990). En la década de los 2000 se descubrieron nuevas familias de GTPasas relacionadas con funciones no clásicas como la biogénesis ribosomal y la biogénesis de proteínas de membrana (Leipe et al., 2002). También se describieron GTPasas cuya función no estaba limitada únicamente a la señalización, sino que participan en el ensamble de estructuras macromoleculares, demostrando que el papel del GTP no se limita a la señalización, sino que participa también en la coordinación de ensambles macromoleculares como en el caso de la GTPasa Gpn1, descrita como una proteína asociada a la RNAPII (Jerónimo et al., 2007) y posteriormente mostrado que era esencial para la localización nuclear de esta enzima (Forget et al., 2010).

1.2 Familia de GTPasas GPN.

La ampliación del conocimiento funcional y estructural de las GTPasas derivó en la identificación de nuevos grupos con funciones celulares esenciales, pero con mecanismos menos convencionales de regulación y localización. Esta diversificación funcional llevó al descubrimiento de la familia GPN, caracterizada por un motivo altamente conservado conformado por los residuos de glicina (G), prolina (P), y asparagina (N), localizado en el dominio G, y esencial para la estabilización del fosfato post hidrólisis. En 2007, se propuso por primera vez llamar a esta familia como "*GPN-loop GTPases*" al caracterizar la única proteína GPN descrita en arqueas hasta ese momento, y describir el motivo GPN conservado, lo que permitió sugerir su posible implicación en procesos celulares esenciales (Gras et al., 2007). Esta familia incluye a las GTPasas humanas Gpn1, Gpn2, Gpn3; mientras que Npa3 en la levadura *Saccharomyces cerevisiae* es el ortólogo de Gpn1. Los tres genes GPN están universalmente conservados en células eucariotas y son esenciales (Forget et al., 2010; Carre & Shiekhattar, 2011; Staresincic et al., 2011). En arqueas, se conoce una copia única del gen GPN (Alonso et al., 2013). Análisis filogenéticos demostraron que las GTPasas GPN son proteínas altamente conservadas y que están ausentes en bacterias y ciertas arqueas, lo que sugiere un papel crucial en procesos nucleares exclusivos en células con núcleo (Matte-Tailliez et al., 2000; Alonso et al., 2013). Puntualmente, Forget et al., 2010 demostraron que Gpn1 (anteriormente denominada RPAP4/XAB1) es fundamental para la importación nuclear del complejo multienzimático de la RNAPII, la enzima responsable de la transcripción de todos los mRNA, vinculando por primera vez de manera funcional a una GTPasa GPN con la maquinaria de transcripción en células eucariotas. Este hallazgo consolidó la idea de que las GTPasas GPN actúan como factores de ensamble y maduración del complejo de la RNAPII y no como proteínas de señalización. Estudios posteriores realizados por Forget et al. en 2010 y Minaker et al. en 2013, mostraron que las GTPasas GPN funcionan de manera interdependiente contribuyendo en el ensamble e importación de la RNAPII al núcleo. Estructuralmente, el primer cristal fue obtenido a partir de la proteína PAB0955 de *Pyrococcus abyssi*, una arquea hipertermófila. La estructura se resolvió

en su forma unida a GDP, en ausencia de iones de magnesio. PAB0955 fue reportada como un homodímero estable. Posteriormente, fue resuelta la estructura cristalográfica de Npa3 (Niesser et al., 2016), proporcionado información crucial sobre su función en la biogénesis de la RNAPII. Se demostró que Npa3 existe en dos conformaciones, una cerrada unida a GDP, y otra abierta unida a un análogo no hidrolizable de GTP (GMPPCP). Por otro lado, Npa3 mostró una cavidad hidrofóbica exclusivamente en la conformación abierta, alejada del sitio de unión a los nucleótidos de guanina. Se propuso que, a través de esta cavidad, Npa3 es capaz de interactuar con regiones de péptidos hidrofóbicos en la superficie de las subunidades de la RNAPII, sugiriendo un papel de esta GTPasa como chaperona en el ensamble del complejo enzimático de la enzima.

La RNAPII es un complejo formado por 12 subunidades (Rpb1-Rpb12), las cuales han sido extensamente estudiadas (Wild & Cramer, 2012). El núcleo catalítico está compuesto por 10 subunidades, el cual está organizado en tres subensambles: el subensamble Rpb1 que incluye a las subunidades Rpb1, Rpb5, Rpb6, y Rpb8; el subensamble Rpb2, formado por Rpb2 y Rpb9 y por el subensamble Rpb3, que consta de Rpb3, Rpb10, Rpb11, y Rpb12. Para la formación del complejo entero de la RNAPII son necesarios varios pasos intermediarios y factores de ensamblaje (Boulon et al., 2010; Wild & Cramer, 2012). Una propuesta importante del trabajo de Niesser (Niesser et al., 2016), fue que la interacción entre los péptidos en la superficie de las subunidades de la RNAPII, y Npa3 en conformación abierta mediante su cavidad hidrofóbica estimula alostéricamente la actividad de GTPasa y facilita la liberación posterior de los péptidos, proceso indispensable para la maduración y movilización de la RNAPII al núcleo.

Estos hallazgos, además de evidenciar la función de Npa3 como chaperona molecular, también reflejan la conservación estructural y funcional de las GTPasas GPN en eucariotas. Finalmente, la presencia del motivo GPN altamente conservado y de mecanismos alostéricos de regulación demuestran su papel esencial en la organización, ensamblaje y estabilidad de la RNAPII, situando a la familia de GTPasas GPN como componentes clave en la organización y regulación de procesos nucleares necesarios que sustentan la viabilidad celular.

1.3. Métodos computacionales en el estudio de interacciones moleculares

El estudio de las interacciones moleculares es esencial para comprender los procesos biológicos a nivel atómico. La identificación de los mecanismos de reconocimiento y asociación específica de moléculas como proteínas, ácidos nucleicos, lípidos y otras moléculas pequeñas permiten dilucidar procesos biológicos complejos como la señalización celular y la catálisis enzimática, entre otros (Goodsell & Olson, 2000; De Vivo et al., 2016; Chen et al., 2024). El soporte original para el estudio de estos mecanismos, han sido las técnicas experimentales de la cristalografía de rayos X, la resonancia magnética nuclear (RMN) y más recientemente, la criomicroscopía electrónica (crio-EM) (Son et al., 2024).

En adición a esta variedad de técnicas de resolución de estructuras, la disponibilidad del poder computacional actual y el desarrollo de modelos teóricos avanzados han impulsado fuertemente la integración de métodos computacionales como herramientas complementarias al estudio de la biología estructural. Estos enfoques permiten explorar, con resolución atómica, las bases fisicoquímicas del reconocimiento molecular y la dinámica de las macromoléculas biológicas (Nussinov et al., 2019; Frasnetti et al., 2024; Zhang & Qian, 2024). Las técnicas computacionales más empleadas en biología estructural incluyen el acoplamiento molecular (*molecular docking*), las simulaciones de dinámica molecular y los métodos de modelado por homología o predicción estructural, como el caso de AlphaFold en los últimos años (Miyazono & Tanokura, 2022; Zhu et al., 2022; Li, 2024). Cada una de estas técnicas ofrece una perspectiva distinta hacia el entendimiento de cómo los sistemas biológicos moleculares interactúan y se organizan. La aplicación de estas técnicas computacionales, en combinación con datos experimentales ha demostrado ser una poderosa estrategia para la formulación de hipótesis sobre los mecanismos específicos del funcionamiento de proteínas, así como para la identificación de moléculas con potencial terapéutico. En consecuencia, los enfoques *in silico* no solo complementan los datos estructurales derivados de métodos experimentales, sino que también los enriquecen proporcionando una visión más detallada y realista de la dinámica molecular.

1.4 Acoplamiento molecular.

Se han estudiado extensamente los requisitos para la búsqueda de moléculas con actividad biológica, enfatizando la importancia de un análisis detallado del receptor, el estudio de las propiedades de sus cavidades, y la caracterización de aquellas con potencial farmacológico (Walters & Murcko, 2002; An et al., 2004; Pérot et al., 2010; Hughes et al., 2011; Ru et al., 2024). El acoplamiento molecular o *molecular docking* es un enfoque bioinformático que permite predecir la orientación y afinidad con la que una molécula pequeña o ligando interactúa con un sitio activo o de unión sobre la superficie una proteína, así como en la generación de complejos proteína-proteína o proteína-péptidos (Kuntz et al., 1982; Kitchen et al., 2004; Fink et al., 2009; Mondal et al., 2022). Este método combina información estructural de la proteína y del ligando con algoritmos de búsqueda y *scoring,* donde se estima la geometría y las contribuciones energéticas de la interacción, cuyo objetivo es la identificación de las configuraciones más favorables (Lengauer & Rarey, 1996; Pagadala et al., 2017). Se ha convertido en una herramienta fundamental en los estudios moleculares al permitir la exploración y descripción detallada de interacciones proteína-ligando o proteína-proteína, facilitando la identificación de moléculas potencialmente inhibidoras o moduladoras (Kitchen et al., 2004; Meng et al., 2011). Por otro lado, complementa estudios estructurales y funcionales mediante la formulación de propuestas de mecanismos teóricos sobre la dinámica de las interacciones moleculares de las proteínas (Goodsell & Olson, 1990; De Vivo et al., 2016; Mondal et al., 2022). A pesar de décadas de estudio sobre interacciones moleculares, los métodos clásicos de *docking* consideran usualmente a la proteína como una estructura rígida, limitando su capacidad para representar los movimientos y cambios conformacionales inherentes a su función biológica. Así, considerando que las proteínas son entidades dinámicas cuyas conformaciones fluctúan, surge la necesidad de incorporar flexibilidad en los modelos de acoplamiento (Ferreira et al., 2015; Harmalkar & Gray, 2021). En este contexto, el acoplamiento flexible se ha desarrollado como una extensión de los enfoques tradicionales, permitiendo la exploración de múltiples conformaciones tanto del ligando como del sitio activo de la proteína (Lee et al., 2025). La exploración

considera el grado de flexibilidad de las moléculas que interactúan, sirve como complemento a los estudios estructurales y funcionales, buscando ofrecer una aproximación más cercana a un contexto biológico real de los mecanismos de reconocimiento molecular y posibles modos de unión (Erickson et al., 2004; Grassmann et al., 2024).

En el presente estudio, se exploró la cavidad hidrofóbica en la forma abierta (unidos a GTP) de Npa3 y en el modelo de Gpn1 con la finalidad de obtener información sobre sus propiedades estructurales. Basados en estos datos, se realizaron experimentos de acoplamiento flexible proteína-proteína sobre los péptidos de la RNAPII identificados por Niesser et al. (2016) que se unieron con mayor afinidad con el objetivo de modelar estas interacciones *in silico*, brindando información sobre los modos particulares de unión y contactos específicos. Para investigar potenciales inhibidores químicos que afecten la función de estas GTPasas esenciales y comprender sus mecanismos biológicos, se realizaron experimentos de acoplamiento molecular sobre la cavidad hidrofóbica del cristal de Npa3 y el modelo por homología de Gpn1 existente en su conformación abierta en contra de una biblioteca de compuestos aprobados por la FDA. Finalmente, se proponen compuestos que podrían funcionar como inhibidores potenciales para su futura evaluación experimental *in vitro,* así como modelos de la interacción de estas GTPasas con péptidos de la superficie de la RNAPII.

Conjuntando la relevancia biológica de Npa3, en combinación con la existencia de la cavidad hidrofóbica en las estructuras activas, su interacción con péptidos en la superficie de las subunidades de la RNAPII, y el limitado entendimiento de su mecanismo de actividad, Npa3 emerge como un blanco ideal en la búsqueda de inhibidores potenciales químicos capaces de afectar su actividad de chaperona disrumpiendo las interacciones con péptidos clave de las subunidades de la RNAPII, previniendo su ensamble.

2. SECCIÓN ARTÍCULO.

El presente artículo fue publicado en la revista de la Sociedad Americana de Química “ACS Omega”, con el título:

“Proposal of Chemical Inhibitors That Compete with the Binding of RNA Polymerase II Subunits to Essential GTPases GPN Npa3 and Gpn1”

El artículo completo y su material suplementario, puede ser consultado, citado y descargado en el siguiente enlace:

https://doi.org/10.1021/acsomega.5c05849

ACS OMEGA

Open Access

http://pubs.acs.org/journal/acsodf

Article

Proposal of Chemical Inhibitors That Compete with the Binding of RNA Polymerase II Subunits to Essential GTPases GPN Npa3 and Gpn1

Julio A. Muñiz-Luna, Ángel Santiago, Gema R. Cristóbal-Mondragón, Mónica R. Calera,* Roberto Sánchez-Olea,* and Nina Pastor*

Cite This: *ACS Omega* 2025, 10, 52585−52597

Read Online

ACCESS | Metrics & More | Article Recommendations | Supporting Information

ABSTRACT: The Gpn1, Gpn2, and Gpn3 proteins are members of the GTPase GPN family; yeast Npa3 is an orthologue of the human Gpn1 protein. These proteins play a crucial role in the nuclear accumulation of RNA polymerase II, functioning as molecular chaperones. The crystallographic structures of Npa3 reveal open and closed conformations, which are dependent on the bound guanine nucleotide (GMPPCP or GDP, respectively). The open conformation of Npa3 exhibits a hydrophobic pocket proposed to be essential for the recognition and binding of specific peptides of RNA polymerase II, contributing to its biogenesis; however, structural data on these complexes remain unavailable. In this work, we present *in silico* models of the interactions between the crystallographic structure of monomeric Npa3 in its open conformation and yeast RNA polymerase II peptides, generated through flexible computational docking. To identify inhibitors of these interactions, potentially useful in understanding the molecular and cellular functions of these proteins, we performed molecular docking experiments using a designed library of FDA-approved compounds on both the Npa3 structure and a homology model of human Gpn1. Our analysis identified potential inhibitors, including atovaquone for both Npa3 and Gpn1 (docking scores: −14.4 and −13.5 kcal/mol, respectively) and tibolone for Npa3 (−13.6 kcal/mol), following flexible docking optimization. Additionally, our docking models suggest key residues in Npa3 such as F143 and W179, which may be critical for recognizing RNA polymerase II subunits and drug-like molecules. These findings can be further explored through biochemical and mutagenesis studies to assess their roles in RNA polymerase II recognition.

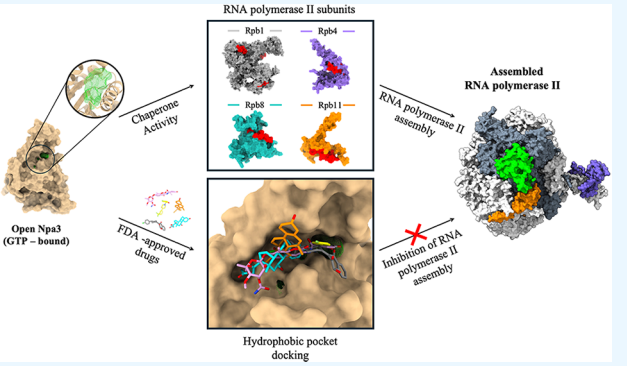

1. INTRODUCTION

GTPases constitute a superfamily of enzymes with the ability to bind guanine nucleotides and hydrolyze GTP, acting as molecular switches and transitioning between inactive (GDP-bound) and active (GTP-bound) conformations. This transition is regulated by guanine nucleotide exchange factors (GEFs) and GTPase activating proteins (GAPs).[1−3] GEFs facilitate the exchange of GDP for GTP, while GAPs promote the hydrolysis of GTP to GDP, leading to an inactive state of the GTPase.[4−8] GTPases share a common structural domain consisting of 170 residues distributed across five motifs (G1 to G5), crucial for GTP binding and hydrolysis.[2,9] During GTP hydrolysis, the γ phosphate is attacked by a nucleophilic water molecule, causing its release, resulting in the GTPase inactive state (GDP-bound). Additionally, there is an apo state, which is an alternative conformation with a disordered switch 1 region.[10] In 2007, Gras et al.[11] proposed the GTPase GPN-loop family, characterized by a highly conserved motif comprising glycine (G), proline (P), and asparagine (N) residues, located in the G domain, essential for stabilizing the phosphate ion posthydrolysis. This family includes human Gpn1, Gpn2, and Gpn3, while Npa3 in yeast (*Saccharomyces cerevisiae*) is the orthologue of Gpn1. In archaea, there is a single copy of the GPN gene. The three GPN genes are universally conserved in eukaryotic cells and indispensable for life.[12,13] Interactions among Gpn1, Gpn2, and Gpn3, leading to heterodimer formation, contribute to their functional roles.[13,14] The crystallographic structure of monomeric Npa3, reported in 2016, reveals two conformations depending on the bound guanine nucleotide: a closed form (GDP-bound) and an open form (GTP-bound, crystallized with a nonhydrolyzable analog of GTP).[15] In addition, the open conformation of Npa3 exhibits an exclusive hydrophobic pocket with a cocrystallized laurate

Received: June 20, 2025
Revised: September 14, 2025
Accepted: September 19, 2025
Published: September 26, 2025

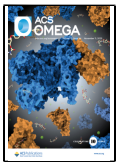

Table 1. Strongest RNA Polymerase II-Interacting Peptides with Npa3[15]

RNA polymerase II subunit	peptide sequence	peptide number	position in the complete subunit	ID UniProt/AlphaFold
Rpb1	FGHIDLAKPVFHVGF	21	81−95	P04050
	KRIAFGFVDRTLPHF	194	773−787	
	ENSYLRGLTPQEFFF	201	801−815	
	YKQLVKDRKFLREVF	234	933−947	
Rpb4	KNTMQYLTNFSRFRD	855	142−156	P20433
Rpb8	LNNLKQENAYLLIRR	1043	132−146	P20436
Rpb11	FAAYKVEHPFFARFK	1109	58−72	P38902

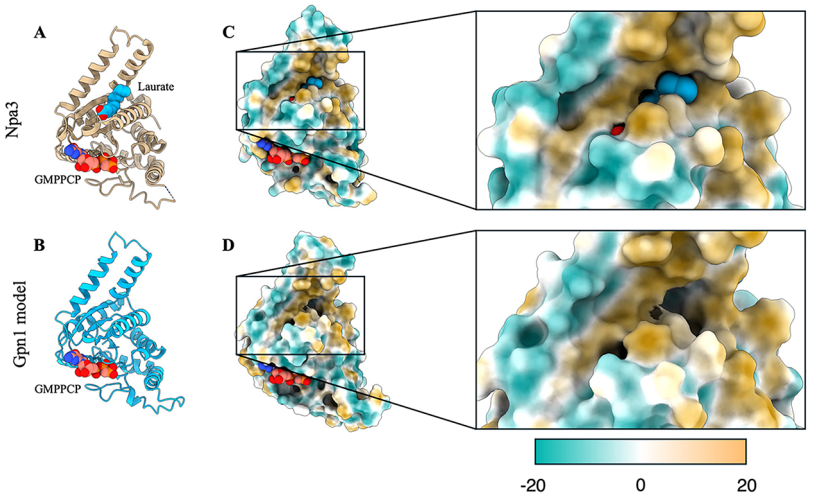

Figure 1. 3D structure of essential GTPases Npa3 and the homology model of human Gpn1 in the open conformation. Cartoon representation of the Npa3 crystal from *S. cerevisiae* (UniProt: P47122; PDB ID: 5HCN) and of the human Gpn1 model (UniProt: Q9HCN4) in the open conformation (GTP-bound, active form) are displayed in sand (A) and blue (B), respectively. Laurate and GMPPCP (nonhydrolyzable analogue of GTP) are displayed as spheres. The hydrophobic (gold) and hydrophilic (cyan) surface representation for Npa3 and Gpn1 is shown in (C, D) in the same orientation as in (A, B), respectively, with the scale bar for the molecular lipophilicity potential (MLP). The magnified area corresponds to the laurate binding site location.

fatty acid molecule, which is not present in the closed conformation.

Npa3/Gpn1 plays a pivotal role in the nuclear accumulation of RNA polymerase II, the enzyme that transcribes all protein-coding genes and some noncoding RNA genes, such as miRNA, lncRNA, and snRNA. The structure of RNA polymerase II, a complex consisting of 12 subunits (Rpb1-Rpb12), has been extensively studied.[12,13,15,16] The catalytic core, composed of 10 subunits, is organized into three subassemblies: the Rpb1 subassembly, which includes Rpb1, Rpb5, Rpb6, and Rpb8 subunits; the Rpb2 subassembly, formed by Rpb2 and Rpb6; and finally, the Rpb3 subassembly containing Rpb3, Rpb10, Rpb11, and Rpb12.[17] The formation of these multisubunit complexes also requires intermediates and assembly factors.[17,18] A model proposed by Niesser et al.[15] suggests that Npa3 can function as a molecular chaperone. This observation stems from qualitative binding assays that indicate that Npa3 interacts through its hydrophobic pocket with key peptides located at the interfaces of RNA polymerase II subunits. These interactions were described to promote the GDP to GTP exchange, proposing an allosteric regulation of nucleotide binding and GTPase activity.

However, understanding the interactions between the hydrophobic pocket of Npa3 and these interface peptides is hampered by a lack of structural information on the complexes. In this sense, computational modeling represents a valuable tool for understanding molecular interactions relevant for protein binding, as well as for the development and identification of bioactive compounds.[19−22] The requirements for searching for small molecules with biological activity have been extensively described by various authors,[23−25] emphasizing the importance of a detailed structural analysis of the receptor, the study of pocket properties, and characterization of those with potentially druggable properties. Computational techniques such as molecular docking are defined as essential tools for predicting models of the interactions between small ligands and macromolecules, as well generating protein−protein or protein−peptide complexes,[21,26−28] offering potential information about specific contacts, interaction energy, binding distances, etc. In this study, we explored the hydrophobic pocket in the open form of Npa3 and human Gpn1 (GTP-bound) in order to obtain information about its structural properties. With this information we performed flexible-type protein−peptide and protein−protein docking against RNA polymerase II peptides identified by Niesser et al.[15] as being strong binders (Table 1), in order to model these interactions *in silico*, providing information on the particular binding modes and specific contacts. To investigate potential chemical inhibitors that affect the function of these essential GTPases and to advance the understanding of their biological mechanisms, we conducted molecular docking experiments in this hydrophobic pocket of Npa3 and the homology model of human Gpn1 against a library of FDA-approved drugs. Finally, we propose potential inhibitors for future experimental evaluation as well as models for the recognition of the interaction of these GTPases with RNA polymerase II peptides. Given the biological relevance of Npa3,

https://doi.org/10.1021/acsomega.5c05849
ACS Omega 2025, 10, 52585−52597

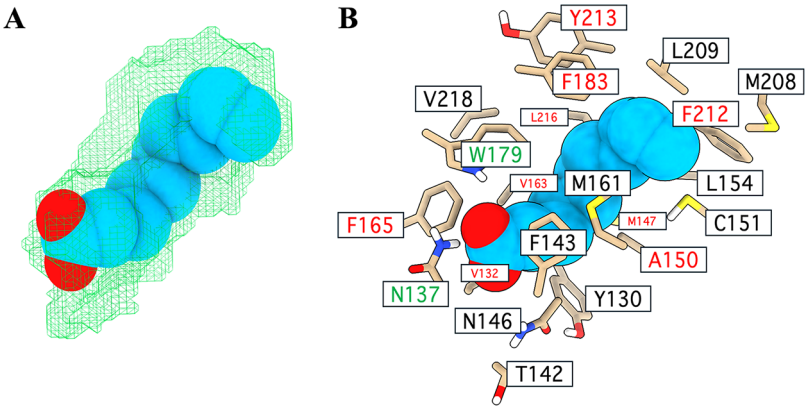

Figure 2. Localization and constituent residues of the "laurate binding site" identified by DoGSiteScorer in the Npa3 structure. (A) Volume of the hydrophobic pocket calculated using the DoGSiteScorer tool shown as a green mesh, with laurate located internally. (B) Constituent residues of the hydrophobic pocket identified by DoGSiteScorer and their positions in relation to laurate.

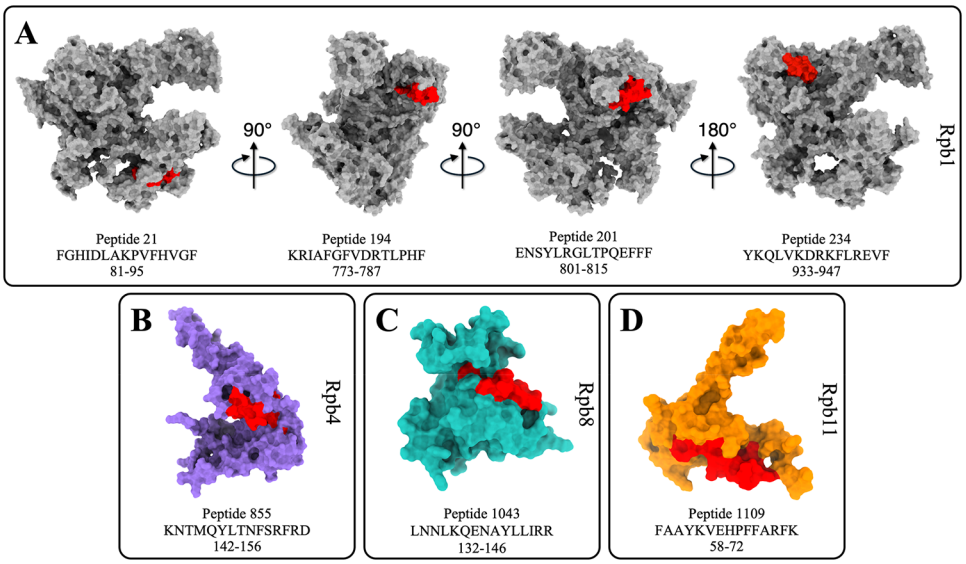

Figure 3. Sequence and localization of peptides used for protein−protein flexible docking. In surface representation are the 15 amino acid peptides from Rpb1 (gray), Rpb4 (purple), Rpb8 (green), and Rpb11 (orange) subunits involved in the interaction with Npa3: (A) Peptides 21, 194, 201, and 234 of Rpb1, (B) 855 of Rpb4, (C) 1043 of Rpb8, and (D) 1109 of Rpb11 are highlighted in red. The position of each peptide within the context of the complete subunit models obtained from AlphaFold2, is indicated below its respective sequence.

in combination with the existence of the hydrophobic pocket, its interaction with the peptides from the interfaces of RNA polymerase II subunits, and the limited understanding of its activity mechanism, Npa3 emerges as an ideal target in the search for potential chemical inhibitors able to affect its chaperone activity by disrupting the interactions with key peptides of RNA polymerase II subunits, preventing its assembly.

2. RESULTS

2.1. Open Npa3 and Human Gpn1 Models Exhibit a Hydrophobic Pocket with Pharmacological Potential. The crystallographic structure of Npa3 and the human Gpn1 model in the open conformation (Figure 1A,B) display the GTPase core fold, characterized by a six-stranded parallel β-sheet surrounded by six α-helices. Notably, the hydrophobic pocket (laurate binding site) is conserved (Figures 1A and S1), suggesting the potential for targeting this conserved site across various species. The surface representation according to hydrophobicity for both the Npa3 and the human Gpn1 model structures are shown in Figure 1C,D, respectively. This pocket is predominantly composed of hydrophobic residues.

To obtain information regarding the localization and properties of this pocket in open Npa3 and Gpn1, we used the bioinformatics tool DoGSiteScorer.[29,30] Notably, the pocket corresponding to the laurate binding site exhibited druggability scores of 0.72 and 0.8 for Npa3 and Gpn1, respectively; values closer to 1 suggest a high probability for acting as a ligand binding site. This score is based on properties such as the pocket volume, surface area, local hydrophobicity, and shape. Figure 2 displays the hydrophobic pocket structure and the surrounding residues. This pocket in the Npa3 structure has a volume of 405.89 A^3, as well as a 0.71/0.29 ratio of nonpolar and polar residues. All hydrophobic pocket descriptors for the Npa3 structure and the Gpn1 model are shown in Table S1. These structural descriptors suggest that the hydrophobic pocket could be a potential druggable target for in-depth study.

2.2. Peptides in the Rpb1, Rpb4, Rpb8, and Rpb11 Subunits Interface Interact *In Silico* with Open Npa3 through Constituent Residues of the Hydrophobic

https://doi.org/10.1021/acsomega.5c05849
ACS Omega 2025, 10, 52585−52597

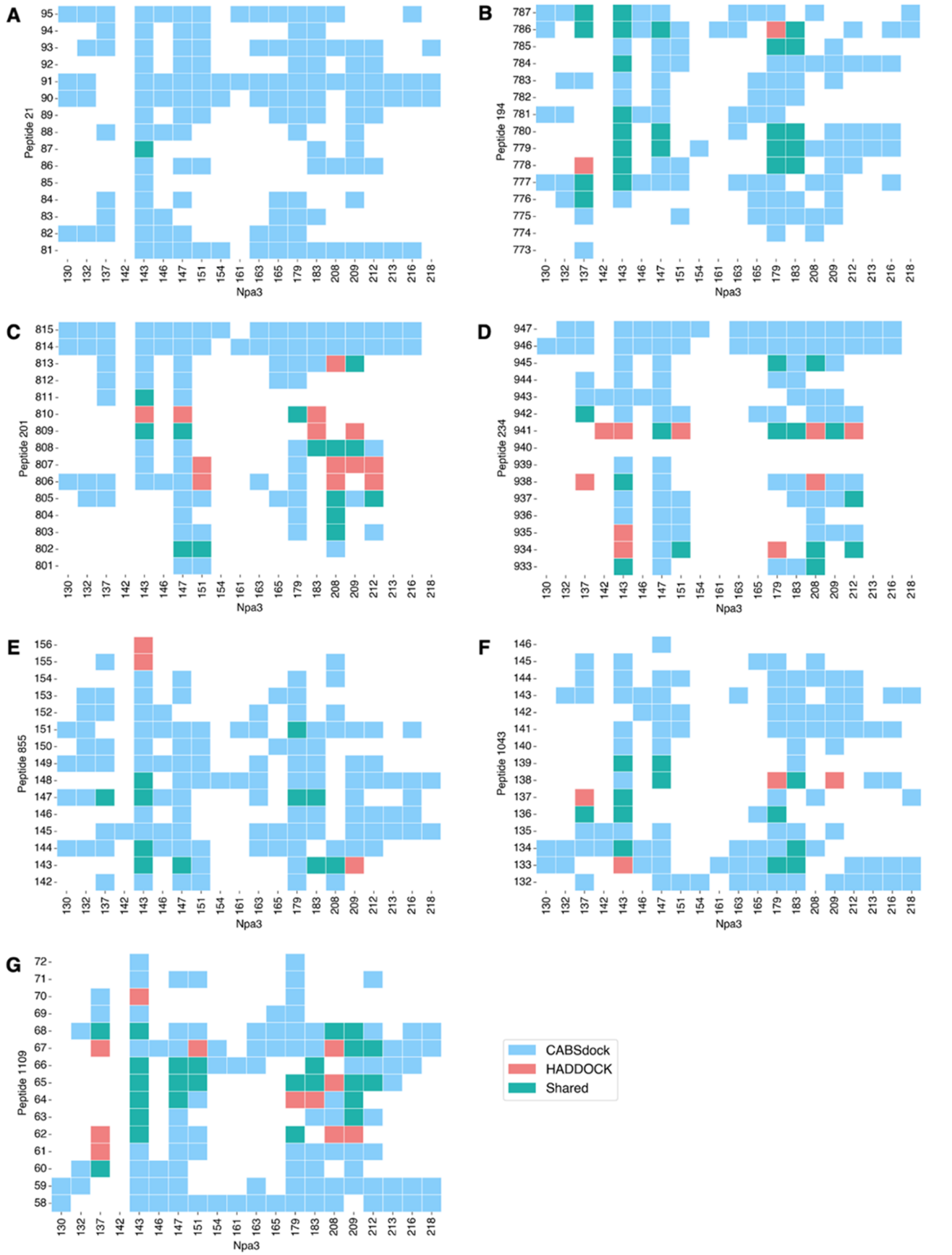

Figure 4. Residue contact heatmap from flexible docking models using CABS-dock and HADDOCK servers. Specific interactions between residues conforming to the hydrophobic pocket of open Npa3 with peptides 21 (A), 194 (B), 201 (C), and 234 (D) from Rpb1; 855 (E) from Rpb4; 1043 (F)

https://doi.org/10.1021/acsomega.5c05849
ACS Omega 2025, 10, 52585−52597

Figure 4. continued

from Rpb8; and 1109 (G) from Rpb11. Contacts present in CABS-dock models are shown in cyan, contacts in HADDOCK models are shown in red, and contacts shared in models from both servers are colored in green. A cutoff threshold of 6 Å was used to define the carbon−carbon contacts.

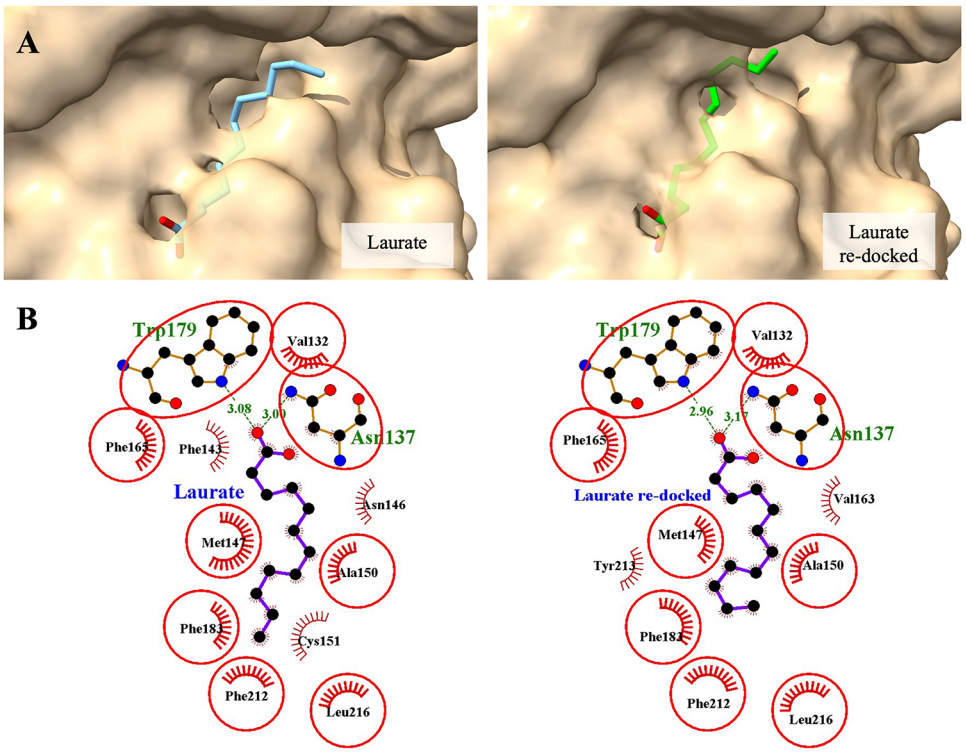

Figure 5. Comparison of laurate binding modes: AutoDock Vina redocking against crystallographic structure of Npa3. (A) The structure of laurate is depicted in blue and green sticks, overlying the Npa3 surface for the crystallographic and redocking pose, respectively. (B) The specific 2D interaction diagrams are shown below.

Pocket. To evaluate the interactions between the Npa3 hydrophobic pocket and peptides from RNA polymerase II subunits displayed in Table 1, models were generated using the CABS-dock[31] and HADDOCK 2.4 servers.[32] The position of each peptide within the context of the complete subunit is displayed in Figure 3 and the AlphaFold2 confidence scores for the predicted structures are shown in Figure S2. Ranking of models generated by CABS-dock and statistics of the HADDOCK score for the clusters generated for each peptide in its respective subunit are presented in Table S2 and Figure S3, respectively.

To evaluate the most prominent interactions in the models generated using the CABS-dock and HADDOCK programs, residue−residue contacts were calculated. Figure 4 presents heatmaps of the consensus residue−residue contacts from the best models, showing the interactions between all selected peptides from the Rpb1, Rpb4, Rpb8, and Rpb11 subunits and the residues comprising the Npa3 hydrophobic pocket. Using a 6 Å cutoff threshold to define carbon contacts, a total of 793 contacts were identified with CABS-dock, 144 with HADDOCK, and 101 shared contacts, i.e., those detected by both HADDOCK and CABS-dock.

Among these interactions, peptide 21 showed the lowest number of shared contacts (in both CABS-dock and HADDOCK): F143 of Npa3 is paired with A87 of Rpb1 (Figure 4A). In contrast, peptide 194 in Rpb1 exhibited 24 shared contacts with Npa3 (Figure 4B), being the second highest. Peptide 1109 from Rpb11 showed the highest number of shared contacts, totaling 25 (Figure 4G). Considering the shared contacts, interestingly, F143 is the only Npa3 residue participating in the interaction with all the studied subunits, both in the context of the complete protein and at the individual peptide level. It participates in a total of 27 shared interactions, based on the evaluation of all peptides, contributing 26.7% of the total shared contacts. On the other hand, it shows 85 contacts according to HADDOCK, representing 24.3% of all the interactions proposed in the context of the complete subunits. In addition, this residue provides the highest number of contacts with a single subunit, a total of eight, including residues F777, G778, F779, V780, R782, L784, H786, and F787 of peptide 194 in Rpb1.

W179 residue in the Npa3 hydrophobic pocket showed the highest participation in shared interactions only behind F143, with a total of 13, establishing contact with all peptides except for 21 in Rpb1. In addition, it contributed the most interactions in the CABS-dock-generated docking, representing 90 of the 793 in total. These findings indicate that F143 and W179 residues may be crucial for the recognition of RNA polymerase II subunits by Npa3.

2.3. Identification of Compounds Docked to the Hydrophobic Pocket of Npa3 and Gpn1. To identify compounds that can function as potential inhibitors of Npa3-RNA polymerase II interactions, as an initial step we performed rigid docking of FDA-approved drugs over the Npa3 laurate

https://doi.org/10.1021/acsomega.5c05849
ACS Omega 2025, 10, 52585−52597

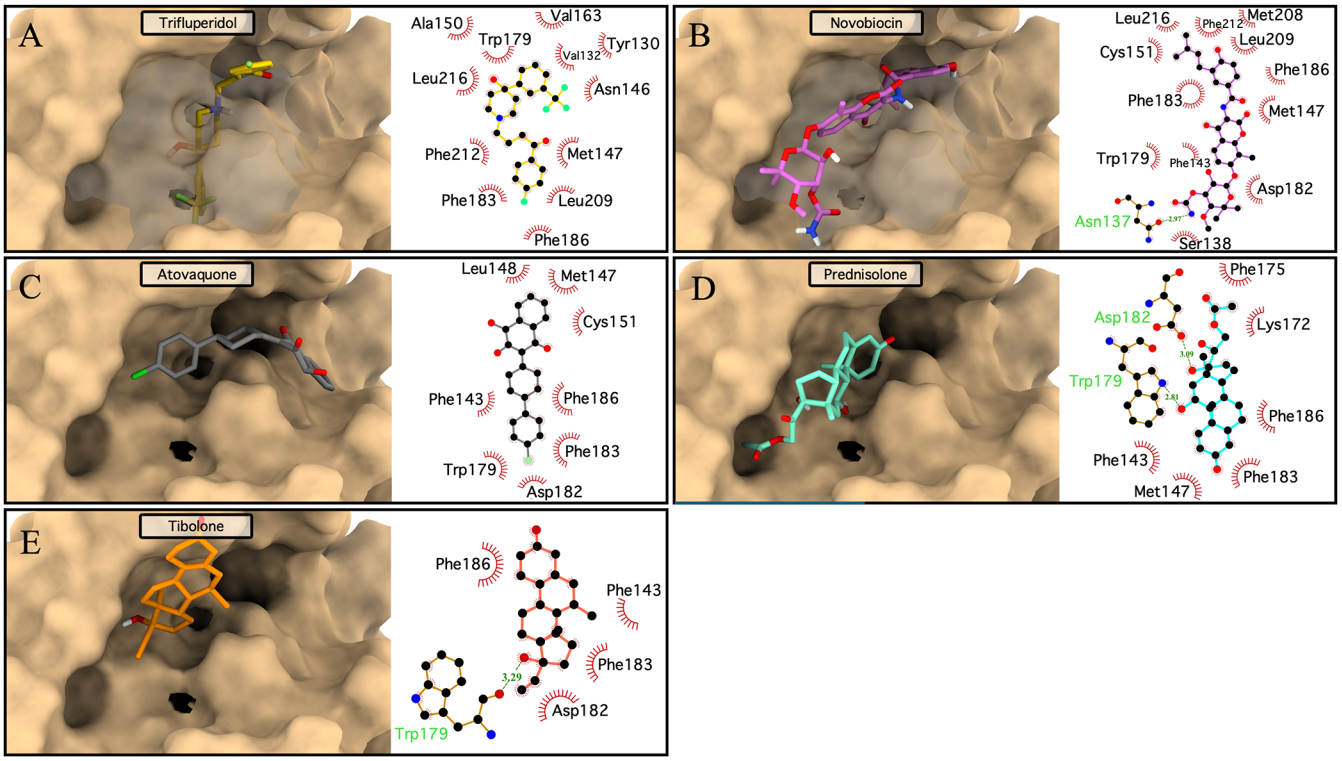

Figure 6. Binding modes from rigid docking and 2D interaction diagrams for the specific contacts between open Npa3 and the five compounds with the best binding energy. Npa3 is shown in sand-colored surface representation, (A) trifluperidol compound docked inside the hydrophobic pocket is shown in yellow, (B) novobiocin shown in pink, (C) atovaquone shown in dark gray, (D) prednisolone in turquoise, and (E) tibolone in orange. For the 2D interaction diagrams, each compound representation corresponds to the assigned color in the 3D view.

Table 2. Top 5 Compounds Docked with Open Npa3 (Rigid Docking)

ZINC ID	ligand	ΔG (kcal/mol)	hydrogen bonding	hydrophobic interactions
ZINC00538505	trifluperidol	−7.9		L216, F212, L209, F186, F183, W179, V163, A150, M147, N146, and V132
ZINC03831234	novobiocin	−7.9	N137	L216, F212, L209, M208, F186, F183, D182, W179, C151, M147, F143, S138, and N137
ZINC12504271	atovaquone	−7.9		F186, F183, D182, W179, C151, L148, M147, and F143
ZINC03831370	prednisolone acetate	−7.8	W179 and D182	F186, F183, D182, W179, F175, L172, M147, and F143
ZINC11616424	tibolone	−7.8	W179	F186, F183, D182, and W179

binding pocket using AutoDock Vina.[33] Previous validation by redocking laurate was performed. AutoDock Vina was able to reproduce the binding orientation of laurate cocrystallized with open Npa3 (Figure 5A), resulting in two hydrogen bonds from N137 and W179 with a laurate carboxylate oxygen (Figure 5B). In the crystal structure, the same two hydrogen bonds are observed between W179 and N137, interacting with a carboxylate oxygen in the fatty acid moiety from laurate. The binding distances for these interactions are 3.08 and 3.0 Å, respectively. In the redocking pose, these distances were 2.96 and 3.17 Å, respectively. F143 displayed hydrophobic interactions with laurate, suggesting that both F143 and W179 are important for ligand recognition. The resulting energy from redocking laurate into Npa3 was −6.1 kcal/mol, whereas that obtained from the Vina rescoring function for the crystallographic structure was −4.9 kcal/mol.

The results of rigid docking for the FDA-approved compound library with the Npa3 and Gpn1 are shown in Figures S4 and S5, respectively, yielding a total of 8,930 model structures. Based on the docking results, the top five compounds with the best scores were selected for analysis. Specific interactions for the top five compounds were evaluated, including trifluperidol, novobiocin, atovaquone, prednisolone, and tibolone (Figure 6). The specific interactions between Npa3 and the five compounds with the best energy are also listed in Table 2. Novobiocin presented the maximum number of hydrophobic interactions with Npa3, with a total of 13. Nine of these interactions were residues of the hydrophobic pocket (F212, L209, M208, F186, F183, D182, C151, M147, and S138), including W179 and F143 as in the CABS-dock and HADDOCK models. It also engages in one hydrogen bond with N137. The interaction energy calculated by AutoDock Vina for this interaction was −7.9 kcal/mol. Notably, trifluperidol was able to dock inside the hydrophobic pocket with an orientation similar to that of laurate, binding to Npa3 predominantly through hydrophobic interactions with an energy of −7.9 kcal/mol. It presented a total of 11 interactions, involving 10 residues from the hydrophobic pocket (Table 2).

The top five compounds with the best binding energy for the Gpn1 model include ketanserin, gliquidone, dicumarol, nefazodone, and atovaquone (Figure 7). The specific interactions among the five compounds analyzed and Gpn1 are included in Table 3. Among these, gliquidone established the

https://doi.org/10.1021/acsomega.5c05849
ACS Omega 2025, 10, 52585−52597

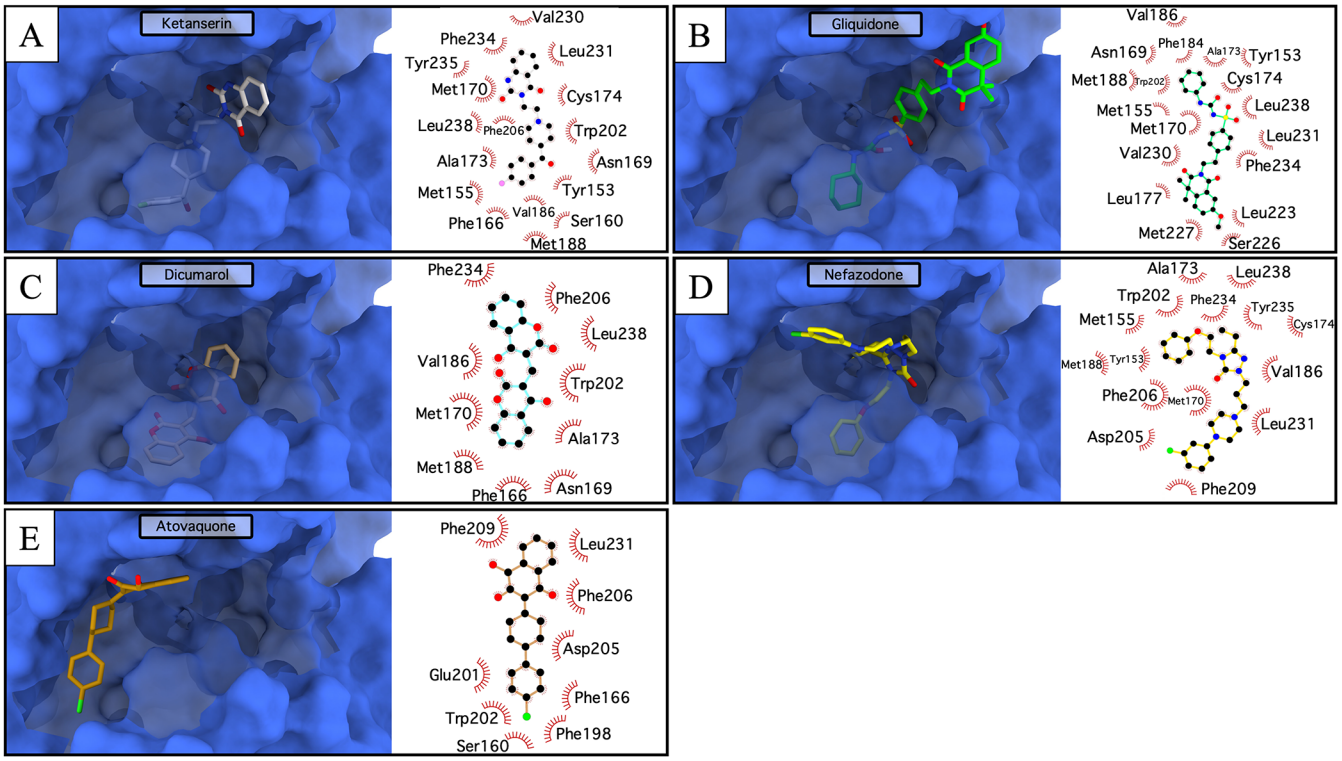

Figure 7. Binding modes from rigid docking and 2D interaction diagrams for the specific contacts between the Gpn1 model in open conformation and the five compounds with the best binding energy. The Gpn1 model is displayed in blue surface representation, while the docking of (A) ketanserin is in white, (B) gliquidone is in lime, (C) dicumarol is in cyan, (D) nefazodone is in yellow, and (E) atovaquone is in dark orange. For the 2D interaction diagrams, each compound representation corresponds to the assigned color in the 3D view.

Table 3. Top 5 Compounds Docked with the Open Gpn1 Model (Rigid Docking)

ZINC ID	ligand	ΔG (kcal/mol)	hydrophobic interactions
ZINC00537877	ketanserin	−9.3	L238, F234, L231, V230, F206, W202, M188, V186, C174, A173, M170, N169, F166, S160, M155, and W153
ZINC01482077	gliquidone	−9.1	L238, F234, L231, V230, M227, S226, L223, W202, M188, V186, F184, L177, C174, A173 M170, N169, M155, and W153
ZINC03869855	dicumarol	−8.8	L238, F234, F206, W202, M188, V186, A173, M170, N169, and F166
ZINC00538065	nefazodone	−8.6	L238, Y235, F234, L231, F209, F206, D205, W202, M188, V186, C174, A173, M170, M155, and Y153
ZINC12504271	atovaquone	−8.6	L231, F209, F206, D205, W202, E201, F198, F166, and S160

Table 4. Interaction Energies Generated by Flexible Protein Docking for the Five Compounds with the Best Rigid Docking Energies, Npa3 and Gpn1

Npa3			Gpn1		
ZINC ID	drug name	ΔG (kcal/mol)	ZINC ID	drug name	ΔG (kcal/mol)
ZINC12504271	atovaquone	−14.4	ZINC12504271	atovaquone	−13.5
ZINC11616424	tibolone	−13.6	ZINC03869855	dicumarol	−12.4
ZINC00538505	trifluperidol	−10.8	ZINC01482077	gliquidone	−11.3
ZINC03831370	prednisolone	−9.6	ZINC00537877	ketanserin	−10.3
ZINC03831234	novobiocin	−8.7	ZINC00538065	nefazodone	−9.4

highest number of interactions, totaling 18. The interacting residues include L238, F234, L231, V230, M227, S226, L223, W202, M188, V186, F184, L177, C174, A173 M170, N169, M155, and Y153. Gliquidone docks inside the hydrophobic pocket using the sulfonylurea group, while the remaining molecule extends outside the pocket. Notably, gliquidone displays interactions mapping the portion of hydrophobic pocket such as L238, F234, L231, V230, W202, M188, V186, F184, L177, C174, A173, M170, and N169. For ketanserin, the 2-[4-(4-(*p*-fluorobenzoyl) piperidin-1-yl)ethyl] group was inserted inside the pocket, while the quinazoline group was located at the pocket entrance. It exhibits a total of 16 hydrophobic interactions, involving L238, F234, L231, V230, F206, W202, M188, V186, C174, A173, M170, N169, F166, S160, M155, and Y153. It is noteworthy that only the last two are not considered components of the pocket. Dicumarol, on the other hand, was completely bound inside the pocket, involving 10 hydrophobic interactions with L238, F234, F206, W202, M188, V186, A173, M170, N169, and F166, all residues belonging to the hydrophobic pocket. Similarly, atovaquone

https://doi.org/10.1021/acsomega.5c05849
ACS Omega 2025, 10, 52585−52597

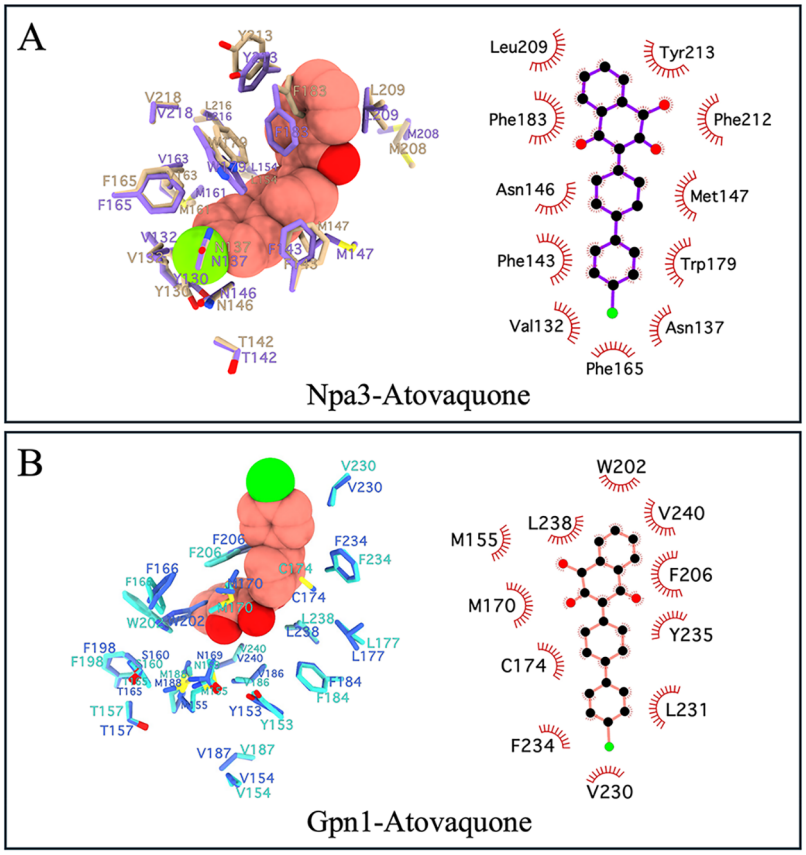

Figure 8. Flexible docking of atovaquone inside the hydrophobic pocket of open Npa3 and Gpn1. Atovaquone is displayed as spheres in salmon color. (A) For docking on the Npa3 structure, the side chains of residues indicated as flexible are colored in sand and are shown as sticks; the position after docking is shown in purple. For docking on the Gpn1 model in (B), the side chains established as flexible are shown in royal blue, whereas in its postdocking position they are colored in cyan. Shown to the right of each 3D representation are the 2D interaction diagrams. Hydrophobic interactions between the flexible Npa3 and Gpn1 model residues, with atovaquone following flexible docking, are indicated in red tabs.

Table 5. Cross-Docking Interaction Energies of Top Compounds from Flexible Docking between Npa3 and Gpn1

Npa3			Gpn1		
ZINC ID	drug name	ΔG (kcal/mol)	ZINC ID	drug name	ΔG (kcal/mol)
ZINC03869855	dicumarol	−12	ZINC11616424	tibolone	−12.6
ZINC01482077	gliquidone	−9.9	ZINC00538505	trifluperidol	−12
ZINC00537877	ketanserin	−13	ZINC03831370	prednisolone	−9.5
ZINC00538065	nefazodone	−10.2	ZINC03831234	novobiocin	−9.4

displayed hydrophobic interactions with external residues of the hydrophobic pocket in Npa3 and Gpn1. Eight contacts were identified with Npa3 and nine with Gpn1. Atovaquone exhibits common interactions for rigid docking in both structures, involving residues F143, C151, W179 and F183 in Npa3, and its equivalents F166, C174, W202 and F206 in Gpn1.

Ketanserin, atovaquone, and dicumarol displayed interactions with F166 and W202 residues from the Gpn1 model, which are the equivalent residues F143 and W179 in the Npa3 structure, and they also were representative residues in all the analyzed models from CABS-dock and HADDOCK.

To account for the flexibility of protein, we conducted an additional refinement step of flexible docking. Binding energies resulting from flexible docking for trifluperidol, novobiocin, atovaquone, prednisolone, and tibolone on Npa3; and for ketanserin, gliquidone, dicumarol, nefazodone, and atovaquone with Gpn1 are shown in Table 4. In all cases flexible docking improves the energy score, suggesting better interactions of each compound with the proteins. Interestingly, the compound that exhibited the highest interaction energy in both Npa3 and Gpn1 was atovaquone, resulting in −14.4 and −13.5 kcal/mol for Npa3 and Gpn1, respectively. Figure 8 details the specific interactions between the two proteins and atovaquone as well as the changes in the position of the side chains for the flexible residues. As can be appreciated in Figure 8, the improved energy score for atovaquone is related to a more relaxed position of the side chains in the hydrophobic residues.

Given the similarity in the pockets of Npa3 and Gpn1, it was surprising that only atovaquone was shared as the best ligand. To explore further the equivalence of the binding pocket in both proteins, we carried out flexible docking of the nonshared top five compounds in the other protein, with the same docking protocol. The resulting energies are presented in Table 5.

These ligands exhibit comparable binding energies in both proteins; the largest differences are found for trifluperidol (1.2 kcal/mol better for Gpn1), gliquidone (1.4 kcal/mol better for

https://doi.org/10.1021/acsomega.5c05849
ACS Omega 2025, 10, 52585−52597

Gpn1), and ketanserin (2.7 kcal/mol better for Npa3). Furthermore, the binding energies are within the range of those in Table 4. Taken together, these results suggest that both binding pockets are equivalent and that these nine compounds are good candidates as inhibitors for either protein.

3. DISCUSSION

The essential GTPases human Gpn1 and its yeast orthologue Npa3 in *S. cerevisiae* play a crucial role in the nuclear accumulation of RNA polymerase II.[12,13,15,16] Despite their importance, the precise mechanism underlying their functions remains elusive. Npa3 in the open conformation features a hydrophobic pocket ("laurate binding site") proposed to be relevant for the binding of peptides from RNA polymerase II subunits in biochemical experiments.[15] In this work, we use a combination of computational techniques to evaluate the possible interactions of Npa3 and Gpn1 GTPases with RNA polymerase II subunit peptides experimentally evaluated by Niesser et al.[15] and propose potential inhibitors of their RNA polymerase binding function, for future experimental evaluation.

The availability of the Npa3 crystallographic structure[15] allowed the generation of a human Gpn1 model that revealed the conservation of this hydrophobic pocket (Figures 1 and S1). Pocket analysis with DoGSiteScorer shows that the pocket containing the cocrystallized laurate fatty acid, i.e., the hydrophobic pocket proposed as the peptide binding site, has the highest volume and score in both Npa3 and Gpn1 models (Figure 2 and Table S1). In addition, its druggability score is particularly important, considering that a higher druggability score is associated with a higher pharmacological potential of the pocket. In this sense, the druggability value was considered acceptable and was an indicator that the pocket exhibits advantageous characteristics, including an appropriate volume, accessibility, and physicochemical properties that make it suitable for ligand binding. Additionally, the laurate molecule cocrystallized in the open conformation of Npa3 structure is particularly crucial because it acts as a pocket marker, i.e., it binds to a potentially pharmacological site in the protein, correlating with the DoGSiteScorer results.

On the other hand, the CABS-dock and HADDOCK servers were a valuable instrument to determine the specific contacts between Npa3 and the peptides of the Rpb1, Rpb4, Rpb8, and Rpb11 subunits. This information is especially useful, given that no three-dimensional models are available for these interactions, which could be essential for the nuclear import of the RNA polymerase II complex. Flexible protein−peptide and protein−protein docking was performed with CABS-dock and HADDOCK 2.4 servers to evaluate the interaction of RNA polymerase II peptides with Npa3 through its hydrophobic pocket as individual peptide and in the conformations found in the full-length and folded subunits obtained from AlphaFold2 (Figures 3 and S2). Residues most frequently involved in the interactions modeled by both servers were F143, W179, and N137 (Figure 4). Overall, the number of interactions generated by individual peptides in CABS-dock models was approximately 5.5 times larger than those observed in HADDOCK, i.e., in the context of full-length subunits. These differences can be attributed to better accessibility of Npa3 to the subunit peptides in CABS-dock models, in contrast to the fully assembled RNA polymerase II subunits in HADDOCK models. Particularly for Rpb1 peptide 21 contacts, the best HADDOCK clusters revealed a single interaction between F143 of Npa3 and A87 in Rpb1; the limited interactions observed were a consequence of the presence of two α-helices located around the peptides defined as active for docking, decreasing the accessibility for Npa3. F143 contributes approximately a quarter of all interactions defined in consensus by CABS-dock and HADDOCK, representing the most crucial interaction in all HADDOCK docking results. F143 also participates in laurate binding in the crystal (Figure 5). In our docking studies in the Npa3 structure, this residue shows participation in the binding of chemical compounds, such as novobiocin, atovaquone, prednisolone, and tibolone (Figure 6 and Table 2). For Gpn1, the equivalent residue corresponds to F166 (Figure S1) and participates in the interaction with ketanserin, dicumarol, and atovaquone (Figure 7 and Table 3). W179, in turn, is the second highest participant in the interactions shared by CABS-dock and HADDOCK (Figure 4). In the Npa3 structure and Gpn1 model, it establishes a hydrogen bond with the laurate carboxylate, contributing to its binding and stabilization inside the hydrophobic pocket. In the docking of FDA-approved drugs, W179 (W202 in Gpn1) was involved in the binding of trifluperidol, novobiocin, prednisolone, and tibolone in Npa3, through hydrophobic interactions and hydrogen bonds (Figures 6 and 7). In Gpn1 its equivalent residue, W202, interacts hydrophobically with ketanserin, gliquidone, dicumarol, nefazodone, and atovaquone. Based on this information, we consider that residues F143 and W179 from the hydrophobic pocket in Npa3 could play a critical role in the recognition of RNA polymerase II subunits and drug-like molecules. These residues could be proposed to be evaluated by mutagenesis experiments to understand their role in the Npa3 function.

Other residues involved in the interaction of Npa3 with the evaluated ligands and the peptides at the interface of the RNA polymerase II subunits include F212 which contributes to the binding of trifluperidol and novobiocin and also interacts with peptides 201 and 234 in Rpb1 (Figures 4 and 6). Also, F183 participates in all evaluated interactions, with the above-mentioned exception of peptide 21, binding to Rpb1, Rpb4, Rpb8, and Rpb11, as well as to the top five compounds in the library.

In this study the presence of laurate cocrystallized with Npa3 inside the pocket was taken as a guide to validate the docking protocol with AutoDock Vina. The capability of AutoDock Vina to reproduce the laurate orientation inside the hydrophobic pocket indicates that AutoDock Vina was suitable for ligand docking of the FDA-approved drugs in Npa3 and human model Gpn1 (Figure 5).

The rigid docking of the FDA-approved compounds resulted in novobiocin docked in the external portion of the hydrophobic pocket (Figure 6B), having the highest energy together with trifluperidol and atovaquone (Figure 6A,C, respectively). Novobiocin belongs to the aminocoumarin family and is an inhibitor of bacterial DNA synthesis by acting on DNA gyrase B.[34] A precedent involving interaction between novobiocin and a molecular chaperone has been reported previously.[35] They showed that this antibiotic binds to the C-terminal domain of the heat shock protein Hsp90, interfering with the association of the cochaperones Hsc70 and p23, causing its inhibition. In a previous work of the same group,[34] it was reported that novobiocin binds to the ATP recognition site on gyrase B, competing with nucleotide binding. Furthermore, Hocker et al. demonstrated by molecular docking with AutoDock Vina, molecular dynamics simulations, and *in vitro* experimentation that the bicyclic diterpenoid lactone, andrographolide and its derivatives, bind to pockets in the small GTPase K-Ras,

https://doi.org/10.1021/acsomega.5c05849
ACS Omega 2025, 10, 52585−52597

inhibiting GDP-GTP exchange and consequently its oncogenic signal.[26]

Finally, with respect to flexible docking, we found a global increase in the interaction energies of trifluperidol, novobiocin, atovaquone, prednisolone, and tibolone on Npa3; and ketanserin, gliquidone, dicumarol, nefazodone, and atovaquone for the human Gpn1 model (Table 4 and Figure 8). These energy changes are probably the result of the induced fit allowed by flexible docking in contrast to rigid docking.

The flexible docking results (Table 4) revealed an overlap between Npa3 and its human homologue Gpn1, with atovaquone consistently ranking among the top binders for both proteins, suggesting a conserved binding preference. To further assess the specificity of the remaining top compounds, cross-docking was performed with the four nonshared ligands (Table 5). This analysis showed that all of these molecules exhibited favorable and comparable predicted affinities across both proteins. These findings suggest that beyond atovaquone, additional candidate ligands may display cross-reactivity within the GPN family, underscoring their potential as novel inhibitors of the RNA polymerase recognition site in GPN proteins and warranting further experimental validation.

Furthermore, it is plausible to consider that the binding of small molecules inside the hydrophobic pocket, or externally, potentially affect the recognition or hydrolysis of GTP, in agreement with the allosteric pocket model,[36] suggesting the existence of pockets located in distinct sites from the catalytic one with affinity to small molecules, where their binding affects the function of the enzyme. Similarly, GTP/GDP binding can be affected by the interaction of key peptides from the interface of RNA polymerase II subunits with the constituent residues of the open Npa3 hydrophobic pocket. Also, it is essential to study the possible effect of these peptides on the GTPase activity of these essential enzymes. For this purpose, González-González et al.[37] reported in 2017 a protocol for the purification of recombinant human Gpn1, allowing in the near future the assessment of the effect of these compounds *in vitro*.

4. CONCLUSIONS

In this work, we characterized the hydrophobic pocket in Npa3 proposed as essential for the recognition and binding of peptides at the interface of RNA polymerase II subunits Rpb1, Rpb4, Rpb8, and Rpb11. Based on this biochemical information, we modeled by flexible protein−peptide and protein−protein docking the interactions between the essential GTPase Npa3 from the yeast *S. cerevisiae* and the Rpb1, Rpb4, Rpb8, and Rpb11 subunits of the RNA polymerase II multienzyme complex. We identified the specific interactions between key residues of both Npa3 and these subunits. Additionally, we performed rigid molecular docking experiments between Npa3 and homology-modeled human Gpn1 against a library of FDA-approved compounds. In a second round of flexible docking, we determined the residues of both proteins that are most actively involved in interactions against the five chemical compounds with the highest interaction energy, resulting from the first rigid docking. For both GTPases, Gpn1 and Npa3, the top compound in common was atovaquone, exhibiting interaction energies of −7.9 and −8.6 kcal/mol, respectively. Based on the results of flexible molecular docking, we propose the compounds atovaquone, tibolone, ketanserine, dicumarol, and trifluperidol as potential allosteric inhibitors of the chaperone activity of Npa3 in the recognition of RNA polymerase II. The biological relevance of residues F143 and W179 in Npa3; and its equivalents F166 and W202 in Gpn1, which were constantly involved in interactions with the evaluated Rpb1 peptides and small molecules, requires additional examination by site-directed mutagenesis in future experiments. Based on these findings, we propose that these are key residues for the interaction of these GTPases with RNA polymerase II. We finally suggest these compounds for *in vitro* assays with particular interest in the exploration of their potential impact on the subcellular localization of the RNA polymerase II subunits, both in the yeast *S. cerevisiae* and in mammalian cells.

5. MATERIALS AND METHODS

5.1. Selection and Energy Minimization of Open Npa3. This work was performed on the crystallographic structure of Npa3,[15] the yeast ortholog of human Gpn1, in its open (GTP-bound) conformation. The structure is available in the Protein Data Bank (RCSB-PDB)[38] with the PDB code 5HCN. The cocrystallized ligands with Npa3 include fatty acid laurate, GMPPCP (nonhydrolyzable analog of GTP), glycerol, and Mg^{2+}, which were removed before structure optimization. The structure was minimized using the CHARMM36 potential[39] and the charmm38b1 package.[40] This process involved 50 steepest descent steps for all hydrogen atoms followed by a minimization of 50 conjugate gradient steps for all of the atoms; the purpose of these short energy minimizations is to eliminate clashes introduced by adding hydrogen atoms to the crystal structure. Geometrical and energetic assessments were conducted using Procheck, ProSa, and Molprobity.[41] The final structure was used for subsequent analyses.

5.2. Human Gpn1 Model Generation. Human Gpn1 model was built as described by Cristóbal-Mondragón et al.[42] Briefly, Gpn1 lacking N- and C-terminal regions (amino acids 19−270) was generated by homology modeling using the Modeler 9.19 program.[43] The crystallographic structure of Npa3 in its open conformation was taken as a template. The energy minimization procedure applied to refine the model followed the same method as that described for the Npa3 crystallographic structure. The resulting optimized structure was used for subsequent analyses. All equivalences between the residues that constitute the hydrophobic pocket of Npa3 and Gpn1 are shown in Figure S1.

5.3. Pocket Identification and Hydrophobic Pocket Characterization of Open Npa3 and Gpn1 Models. The global properties of pockets in the structure of open Npa3 and Gpn1 were determined using the bioinformatics tool DoGSiteScorer server from the "Structure-Based Modeling Support Server-ProteinPlus".[29] It was configured for the calculation of pockets and subpockets in the full-length protein as well as for the prediction of the druggability score; values for this parameter are assigned between 0 and 1, the closer to 1 suggests that the cavity has a higher probability for acting as a ligand binding site. Pocket volumes were determined using default parameters in the DoGSiteScorer server. Briefly, DoGSiteScorer employs a grid-based algorithm and a difference-of-Gaussian (DoG) filter to detect potential binding cavities on the protein surface. The volume of each predicted pocket is then computed by counting the grid points comprising that pocket and multiplying by the grid box volume, yielding the pocket volume in cubic Å. The information obtained is presented as pocket descriptors, which include pocket volume, surface area, amino acid composition, hydrophobicity, shape, and others. This information allows the estimation of parameters such as pharmacological potential of the pocket.[30] The hydrophobic surface representations for Npa3

https://doi.org/10.1021/acsomega.5c05849
ACS Omega 2025, 10, 52585−52597

and Gpn1 were generated using the "mlp" command in ChimeraX,[44] with default settings and a coloring range of −20 to 20. Briefly, the "mlp" command calculates Molecular Lipophilicity Potential (MLP) maps for proteins, which are analogous to electrostatic potential maps. In this representation, positive potentials correspond to more hydrophobic areas (colored in dark gold), negative values indicate more hydrophilic areas (colored in dark cyan), while midrange values around 0 represent intermediate lipophilicity (colored in white). We relied on the standard protonation state assumptions from ChimeraX default MLP parameters; the MLP calculation thus reflects the standard charged or uncharged form of each amino acid side chain.

5.4. Flexible Docking between Peptides in the Interface of RNA Polymerase II Subunits with Open Monomeric Npa3. Guided by the biochemical assay performed by Niesser et al.,[15] peptides of 15 amino acids with a reported fluorescence intensity exceeding 4.0 were selected (see Table 1). As a first step, we performed flexible docking of these peptides over the Npa3 structure using the CABS-dock server[31] for flexible protein−peptide docking. The Npa3 structure was directly uploaded to the server, specifying the 15 amino acid sequence of each peptide. No other optional settings were defined on the server. As the second step, we considered the subunits within the context of their complete and folded structures. The full 3D models of *S. cerevisiae* Rpb1, Rpb4, Rpb8, and Rpb11 subunits (UniProt: P04050, P20433, P20436, and P38902, respectively) were obtained from the AlphaFold Protein Structure Database.[45] Confidence intervals for the peptides located in each RNA polymerase II employed are shown in Figure S2. All of the structures were previously minimized following the same protocol described for the Npa3 and Gpn1 model structures. The structure of open Npa3 and the RNA polymerase II subunits were directly uploaded to the HADDOCK (High Ambiguity Driven protein−protein DOCKing) server version 2.4 for flexible protein−protein docking.[32] For Npa3, active residues, i.e., those potentially involved in the interaction with these peptides and mapping the hydrophobic pocket (Y130, V132, N137, T142, F143, N146, M147, C151, L154, M161, V163, F165, W179, F183, M208, L209, F212, Y213, L216, and V218) were selected in all of the following flexible docking experiments, according to the findings from DoGSiteScorer. In the case of each RNA polymerase subunit, the 15 amino acids that showed an interaction with Npa3 in the biochemical assays were defined as active residues (Table 1). All other docking parameters were maintained at default settings provided by the server.

From the complexes generated by the CABS-dock and HADDOCK servers, we selected the best for further analysis. CABS-dock models were chosen based on cluster ranking, considering structures that represent around 50% of the total models generated by the program (marked in red in Table S2). In the case of HADDOCK models, selection was based on HADDOCK energy scores (Figure S3), considering the ensemble of models with energies with overlapping standard deviations for each cluster. For the selected models, we calculated residue−residue contacts between the protein and peptide, using MDAnalysis (Python 3.7).[46] Only carbon atoms were considered, and a distance cutoff threshold of 6.0 Å was applied to define contacts.

The generated contact lists were further filtered to retain those residue−residue contacts between the Npa3 hydrophobic pocket residues (as identified by DoGsiteScorer) and the 15 amino acids from each peptide. Residue−residue contacts were categorized in three groups: (1) exclusive to CABS-dock models, (2) exclusive to HADDOCK models, or (3) shared between both docking methods. Heatmap plots visualizing these interactions were created using Matplotlib (Python 3.7).[47]

5.5. Chemical Library Preparation. The ligand library was designed using the ZINC 12 database for commercially available chemical compounds.[48] Parameters such as oral bioavailability, blood-brain barrier crossing ability, human intestinal absorption, solubility, and low toxicity were assessed by applying Lipinski's rule of 5, except for the molecular weight. Compounds exceeding a molecular weight of 600 g/mol were excluded. The following additional parameters were set: net charge ranging from −5 and 5, rotatable bonds between 0 and 50, polar surface area (Å^2) from 0 to 200, polar desolvation (kcal/mol) from −400 to 1, and apolar desolvation (kcal/mol) between −100 and 40. The selection was focused on the FDA-approved drug catalog, resulting in 1786 compounds based on the search parameters.

5.6. Validation by Laurate Redocking and Rescoring of Cocrystallized Laurate. To validate the suitability of AutoDock Vina performance on this system, we carried out redocking experiments. The Npa3 structure in the open conformation was employed, and cocrystallized laurate was removed. The structure of laurate for redocking was obtained from the ZINC 15 database[49] under ID ZINC1529498 (net charge −1, H donors = 0, hydrogen bridge acceptors = 2, tPSA = 40, rotatable bonds = 10, apolar desolvation = 9.86 and polar desolvation = 43.35). Molecular docking between laurate and Npa3 was performed using AutoDock Vina software, with the laurate molecule defined as flexible while Npa3 was maintained rigid. Box dimensions were based on the hydrophobic pocket location, using a grid spacing of 1 Å and including the total volume of the pocket. Ten binding poses for laurate were indicated using an exhaustivity of 20. Additionally, the binding energy of the cocrystallized laurate was calculated using the AutoDock Vina rescoring function, in order to subsequently be compared with the energy obtained from redocking.

5.7. Molecular Docking of the Chemical Library on the Open Npa3 and Gpn1 Hydrophobic Pocket. An initial molecular docking was performed using AutoDock Vina, involving the designed library of 1786 FDA-approved compounds against the minimized Npa3 and homology-modeled human Gpn1, both in the open conformation. The box size was set to 25 Å for the *x*, *y*, and *z* axes. Five poses for each compound were generated using an exhaustiveness of 20. The structures of Npa3 and Gpn1 were defined as rigid, whereas the compounds from the FDA library were defined as flexible. All proteins and ligands were transformed to the PDBQT format prior to use. Polar hydrogen atoms, partial charges, atom types, and torsional information for flexible ligands were considered during docking. Subsequently, we performed a second flexible receptor docking for the top 5 compounds that presented the best interaction energy in the rigid docking round, according to a cutoff energy criterion established as −7.5 kcal/mol against Npa3 and the human Gpn1 model. Flexible residues for Npa3 and Gpn1 correspond to those from the laurate binding site. The same settings employed in rigid docking were used for the sake of consistency. The five compounds with the best energy were selected for the final analysis. For the top five compounds identified through flexible docking for each protein, we performed additional flexible cross-docking of the nonshared compounds to evaluate their cross-interaction potential with

https://doi.org/10.1021/acsomega.5c05849
ACS Omega 2025, 10, 52585−52597

both proteins. The same flexible docking parameters were applied as previously described. 2D interaction diagrams of specific contacts were generated with LigPlot+ software.[50] The cutoff distance for determining hydrophobic interactions, hydrogen bridges, and salt bridges was set to default values as specified by the software.

■ ASSOCIATED CONTENT

Data Availability Statement

Npa3 and Gpn1 input structures used in the docking experiments, structure of laurate and the redocked complex, FDA library in mol2 format, and top 5 ranked complexes resulting from flexible and docking assays (10.5281/zenodo.17117473).

Supporting Information

The Supporting Information is available free of charge at https://pubs.acs.org/doi/10.1021/acsomega.5c05849.

Descriptors of the laurate binding site (Table S1); ranking of models generated by CABS-dock for Npa3 docking (Table S2); comparison of the hydrophobic pockets in Npa3 and Gpn1 (Figure S1); AlphaFold2 models for the docked peptides (Figure S2); HADDOCK scores of clusters of flexible docking (Figure S3); FDA-approved library bound to Npa3 (Figure S4); and FDA-approved library bound to Gpn1 (Figure S5) (PDF)

■ AUTHOR INFORMATION

Corresponding Authors

Mónica R. Calera − *Instituto de Física, Universidad Autónoma de San Luis Potosí, C.P. 78295 San Luis Potosí, SLP, México*; Email: mcalera@ifisica.uaslp.mx

Roberto Sánchez-Olea − *Instituto de Física, Universidad Autónoma de San Luis Potosí, C.P. 78295 San Luis Potosí, SLP, México*; Email: rsanchez@ifisica.uaslp.mx

Nina Pastor − *Centro de Investigación en Dinámica Celular-IICBA, Universidad Autónoma del Estado de Morelos, 62209 Cuernavaca, Morelos, México*; orcid.org/0000-0001-7755-2936; Email: nina@uaem.mx

Authors

Julio A. Muñiz-Luna − *Instituto de Física, Universidad Autónoma de San Luis Potosí, C.P. 78295 San Luis Potosí, SLP, México*; orcid.org/0009-0002-8035-0985

Ángel Santiago − *Departamento de Salud Perinatal, Instituto Nacional de Salud Pública, 62100 Cuernavaca, Morelos, México*; orcid.org/0000-0002-3957-0970

Gema R. Cristóbal-Mondragón − *Facultad de Medicina, Universidad Nacional Autónoma de México, 04510 Mexico City, CDMX, México*

Complete contact information is available at: https://pubs.acs.org/10.1021/acsomega.5c05849

Notes

The authors declare no competing financial interest.

■ ACKNOWLEDGMENTS

This work was funded by the Consejo Nacional de Humanidades, Ciencias y Tecnologías (Conahcyt, currently SECIHTI) with grant number A1-S-21070 (RSO). We thank Consejo Nacional de Humanidades, Ciencias y Tecnologías (Conahcyt, currently SECIHTI) for supporting JAML by granting a doctoral fellowship with number 784721. G.R.C.-M. was supported by a Postdoctoral Fellowship from DGAPA, Universidad Nacional Autónoma de México (UNAM). We also thank the Laboratorio Nacional de Supercómputo del Sureste de México for providing access to the supercomputing system to perform all computational calculations through project number 202201035N (MRC).

■ REFERENCES

(1) Cherfils, J.; Zeghouf, M. Regulation of Small GTPases by GEFs, GAPs, and GDIs. *Physiol. Rev.* **2013**, *93* (1), 269−309.

(2) Reiner, D. J. Small GTPases. *WormBook* **2018**, 1−65.

(3) Bos, J. L.; Rehmann, H.; Wittinghofer, A. GEFs and GAPs: critical elements in the control of small G proteins. *Cell* **2007**, *129* (5), 865−877.

(4) Bourne, H. R.; Sanders, D. A.; McCormick, F. The GTPase Superfamily: A Conserved Switch for Diverse Cell Functions. *Nature* **1990**, *348*, 125−132.

(5) Quilliam, L. A.; Khosravi-Far, R.; Huff, S. Y.; Der, C. J. Guanine Nucleotide Exchange Factors: Activators of the Ras Superfamily of Proteins. *BioEssays* **1995**, *17* (5), 395−404.

(6) Barrett, T.; Xiao, B.; Dodson, E. J.; Dodson, G.; Ludbrook, S. B.; Nurmahomed, K.; Gamblin, S. J.; Musacchio, A.; Smerdon, S. J.; Eccleston, J. F. The Structure of the GTPase-Activating Domain from P50rhoGAP. *Nature* **1997**, *385* (6615), 458−461.

(7) Geyer, M.; Wittinghofert, A. GEFs, GAPs, GDIs and Effectors: Taking a Closer (3D). *Curr. Opin. Struct. Biol.* **1997**, *7* (6), 786−792.

(8) Soundararajan, M.; Eswaran, J. Atypical GTPases as Drug Targets. *Anti-Cancer Agents Med. Chem.* **2012**, *12* (1), 19−28.

(9) Bourne, H. R.; Sanders, D. A.; McCormick, F. The GTPase Superfamily: Conserved Structure and Molecular Mechanism. *Nature* **1991**, *349*, 117−127.

(10) Verstraeten, N.; Fauvart, M.; Versees, W.; Michiels, J. The Universally Conserved Prokaryotic GTPases. *Microbiol. Mol. Biol. Rev.* **2011**, *75* (3), 507−542.

(11) Gras, S.; Chaumont, V.; Fernandez, B.; Carpentier, P.; Charrier-Savournin, F.; Schmitt, S.; Pineau, C.; Flament, D.; Hecker, A.; Forterre, P.; Armengaud, J.; Housset, D. Structural Insights into a New Homodimeric Self-Activated GTPase Family. *EMBO Rep.* **2007**, *8* (6), 569−575.

(12) Forget, D.; Lacombe, A.-A.; Cloutier, P.; Al-Khoury, R.; Bouchard, A.; Lavallée-Adam, M.; Faubert, D.; Jeronimo, C.; Blanchette, M.; Coulombe, B. The Protein Interaction Network of the Human Transcription Machinery Reveals a Role for the Conserved GTPase RPAP4/GPN1 and Microtubule Assembly in Nuclear Import and Biogenesis of RNA Polymerase II. *Mol. Cell. Proteomics* **2010**, *9* (12), 2827−2839.

(13) Minaker, S. W.; Filiatrault, M. C.; Ben-Aroya, S.; Hieter, P.; Stirling, P. C. Biogenesis of RNA Polymerases II and III Requires the Conserved GPN Small GTPases in *Saccharomyces cerevisiae*. *Genetics* **2013**, *193* (3), 853−864.

(14) Alonso, B.; Beraud, C.; Meguellati, S.; Chen, S. W.; Pellequer, J. L.; Armengaud, J.; Godon, C. Eukaryotic GPN-Loop GTPases Paralogs Use a Dimeric Assembly Reminiscent of Archeal GPN. *Cell Cycle* **2013**, *12* (3), 463−472.

(15) Niesser, J.; Wagner, F. R.; Kostrewa, D.; Mühlbacher, W.; Cramer, P. Structure of GPN-Loop GTPase Npa3 and Implications for RNA Polymerase II Assembly. *Mol. Cell. Biol.* **2016**, *36* (5), 820−831.

(16) Calera, M. R.; Zamora-Ramos, C.; Araiza-Villanueva, M. G.; Moreno-Aguilar, C. A.; Peña-Gómez, S. G.; Castellanos-Terán, F.; Robledo-Rivera, A. Y.; Sánchez-Olea, R. Parcs/Gpn3 Is Required for the Nuclear Accumulation of RNA Polymerase II. *Biochim. Biophys. Acta, Mol. Cell Res.* **2011**, *1813* (10), 1708−1716.

(17) Wild, T.; Cramer, P. Biogenesis of Multisubunit RNA Polymerases. *Trends Biochem. Sci.* **2012**, *37* (3), 99−105.

(18) Boulon, S.; Pradet-Balade, B.; Verheggen, C.; Molle, D.; Boireau, S.; Georgieva, M.; Azzag, K.; Robert, M. C.; Ahmad, Y.; Neel, H.; Lamond, A. I.; Bertrand, E. HSP90 and Its R2TP/Prefoldin-like

Cochaperone Are Involved in the Cytoplasmic Assembly of RNA Polymerase II. *Mol. Cell* **2010**, *39* (6), 912−924.
(19) Shoichet, B. K.; Bodial, D. L.; Kuntz, I. D. Molecular Docking Using Shape Descriptors. *J. Comput. Chem.* **1992**, *13* (3), 380−397.
(20) Nadendla, R. R. Molecular Modeling: A Powerful Tool for Drug Design and Molecular Docking. *Resonance* **2004**, *9* (5), 51−60.
(21) Kharb, M.; Jat, R. K.; Parjapati, G.; Gupta, A. Review on Introduction To Molecular Docking Software Technique in Medicinal Chemistry. *Int. J. Drug Res. Technol.* **2012**, *2* (2), 189−197.
(22) Ferreira, L. G.; Dos Santos, R. N.; Oliva, G.; Andricopulo, A. D. Molecular Docking and Structure-Based Drug Design Strategies. *Molecules* **2015**, *20* (7), 13384−13421.
(23) An, J.; Totrov, M.; Abagyan, R. Comprehensive Identification of "Druggable" Protein Ligand Binding Sites. *Genome Inf.* **2004**, *15* (2), 31−41.
(24) Pérot, S.; Sperandio, O.; Miteva, M. A.; Camproux, A. C.; Villoutreix, B. O. Druggable Pockets and Binding Site Centric Chemical Space: A Paradigm Shift in Drug Discovery. *Drug Discovery Today* **2010**, *15* (15−16), 656−667.
(25) Duhé, R. J. Drug Design. In *Encyclopedia of Cancer*; Schwab, M., Ed.; Springer: Berlin, Heidelberg, 2014; p 1423.
(26) Hocker, H. J.; Cho, K. J.; Chen, C. Y.; Rambahal, N.; Sagineedu, S. R.; Shaari, K.; Stanslas, J.; Hancock, J. F.; Gorfe, A. A. Andrographolide derivatives inhibit guanine nucleotide exchange and abrogate oncogenic Ras function. *Proc. Natl. Acad. Sci. U.S.A.* **2013**, *110* (25), 10201−10206.
(27) Kuntz, I. D.; Blaney, J. M.; Oatley, S. J.; Langridge, R.; Ferrin, T. E. A Geometric Approach to Macromolecule-Ligand Interactions. *J. Mol. Biol.* **1982**, *161* (2), 269−288.
(28) Huang, S. Y.; Zou, X. Advances and Challenges in Protein-Ligand Docking. *Int. J. Mol. Sci.* **2010**, *11* (8), 3016−3034.
(29) Volkamer, A.; Griewel, A.; Grombacher, T.; Rarey, M. Analyzing the Topology of Active Sites: On the Prediction of Pockets and Subpockets. *J. Chem. Inf. Model.* **2010**, *50* (11), 2041−2052.
(30) Volkamer, A.; Kuhn, D.; Rippmann, F.; Rarey, M. Dogsitescorer: A Web Server for Automatic Binding Site Prediction, Analysis and Druggability Assessment. *Bioinformatics* **2012**, *28* (15), 2074−2075.
(31) Kurcinski, M.; Jamroz, M.; Blaszczyk, M.; Kolinski, A.; Kmiecik, S. CABS-dock web server for the flexible docking of peptides to proteins without prior knowledge of the binding site. *Nucleic Acids Res.* **2015**, *43* (W1), W419−W424.
(32) Honorato, R. V.; Trellet, M. E.; Jiménez-García, B.; Schaarschmidt, J. J.; Giulini, M.; Reys, V.; Koukos, P. I.; Rodrigues, J. P. G. L. M.; Karaca, E.; van Zundert, G. C. P.; Roel-Touris, J.; van Noort, C. W.; Jandová, Z.; Melquiond, A. S. J.; Bonvin, A. M. J. J. The HADDOCK2.4 web server: A leap forward in integrative modelling of biomolecular complexes. *Nat. Protoc.* **2024**, *19* (11), 3219−3241.
(33) Trott, O.; Olson, A. J. AutoDock Vina: Improving the Speed and Accuracy of Docking with a New Scoring Function, Efficient Optimization, and Multithreading. *J. Comput. Chem.* **2009**, *31* (2), 455−461.
(34) Maxwell, A. The Interaction between Coumarin Drugs and DNA Gyrase. *Mol. Microbiol.* **1993**, *9* (4), 681−686.
(35) Marcu, M. G.; Chadli, A.; Bouhouche, I.; Catelli, M.; Neckers, L. M. The Heat Shock Protein 90 Antagonist Novobiocin Interacts with a Previously Unrecognized ATP-Binding Domain in the Carboxyl Terminus of the Chaperone. *J. Biol. Chem.* **2000**, *275* (47), 37181−37186.
(36) Stank, A.; Kokh, D. B.; Fuller, J. C.; Wade, R. C. Protein Binding Pocket Dynamics. *Acc. Chem. Res.* **2016**, *49* (5), 809−815.
(37) González-González, R.; Guerra-Moreno, J. A.; Cristóbal-Mondragón, G. R.; Romero, V.; Peña-Gómez, S. G.; Montero-Morán, G. M.; Lara-González, S.; Hernández-Arana, A.; Fernández-Velasco, D. A.; Calera, M. R.; Sánchez-Olea, R. Human Gpn1 Purified from Bacteria Binds Guanine Nucleotides and Hydrolyzes GTP as a Protein Dimer Stabilized by Its C-Terminal Tail. *Protein Expression Purif.* **2017**, *132*, 85−96.
(38) Berman, H. M.; Westbrook, J.; Feng, Z.; Gilliland, G.; Bhat, T. N.; Weissig, H.; Shindyalov, I. N.; Bourne, P. E. The Protein Data Bank. *Nucleic Acids Res.* **2000**, *28* (1), 235−242.
(39) Huang, J.; MacKerell, A. D., Jr. CHARMM36 All-Atom Additive Protein Force Field: Validation Based on Comparison to NMR Data. *J. Comput. Chem.* **2013**, *34* (25), 2135−2145.
(40) Brooks, B. R.; Brooks, C. L.; Mackerell, A. D.; Nilsson, L.; Petrella, R. J.; Roux, B.; Won, Y.; Archontis, G.; Bartels, C.; Boresch, S.; Caflisch, A.; Caves, L.; Cui, Q.; Dinner, A. R.; Feig, M.; Fischer, S.; Gao, J.; Hodoscek, M.; Im, W.; Kuczera, K.; Lazaridis, T.; Ma, J.; Ovchinnikov, V.; Paci, E.; Pastor, R. W.; Post, C. B.; Pu, J. Z.; Schaefer, M.; Tidor, B.; Venable, R. M.; Woodcock, H. L.; Wu, X.; Yang, W.; York, D. M.; Karplus, M. CHARMM: The Biomolecular Simulation Program. *J. Comput. Chem.* **2009**, *30* (10), 1545−1614.
(41) Williams, C. J.; Headd, J. J.; Moriarty, N. W.; Prisant, M. G.; Videau, L. L.; Deis, L. N.; Verma, V.; Keedy, D. A.; Hintze, B. J.; Chen, V. B.; Jain, S.; Lewis, S. M.; Arendall, W. B., III; Snoeyink, J.; Adams, P. D.; Lovell, S. C.; Richardson, J. S.; Richardson, D. C. MolProbity: More and better reference data for improved all-atom structure validation. *Protein Sci.* **2018**, *27* (1), 293−315.
(42) Cristóbal-Mondragón, G. R.; Lara-Chacón, B.; Santiago, Á; De-la-Rosa, V.; González-González, R.; Muñiz-Luna, J. A.; Ladrón-de-Guevara, E.; Romero-Romero, S.; Rangel-Yescas, G. E.; Fernández Velasco, D. A.; Islas, L. D.; Pastor, N.; Sánchez-Olea, R.; Calera, M. R. FRET-Based Analysis and Molecular Modeling of the Human GPN-Loop GTPases 1 and 3 Heterodimer Unveils a Dominant-Negative Protein Complex. *FEBS J.* **2019**, *286* (23), 4797−4818.
(43) Webb, B.; Sali, A. Comparative Protein Structure Modeling Using MODELLER. *Curr. Protoc. Bioinf.* **2016**, No. June, 1−37.
(44) Pettersen, E. F.; Goddard, T. D.; Huang, C. C.; Meng, E. C.; Couch, G. S.; Croll, T. I.; Morris, J. H.; Ferrin, T. E. UCSF ChimeraX: Structure visualization for researchers, educators, and developers. *Protein Sci.* **2021**, *30* (1), 70−82.
(45) Jumper, J.; Evans, R.; Pritzel, A.; Green, T.; Figurnov, M.; Ronneberger, O.; Tunyasuvunakool, K.; Bates, R.; Žídek, A.; Potapenko, A.; Bridgland, A.; Meyer, C.; Kohl, S. A. A.; Ballard, A. J.; Cowie, A.; Romera-Paredes, B.; Nikolov, S.; Jain, R.; Adler, J.; Back, T.; Petersen, S.; Reiman, D.; Clancy, E.; Zielinski, M.; Steinegger, M.; Pacholska, M.; Berghammer, T.; Bodenstein, S.; Silver, D.; Vinyals, O.; Senior, A. W.; Kavukcuoglu, K.; Kohli, P.; Hassabis, D. Highly Accurate Protein Structure Prediction with AlphaFold. *Nature* **2021**, *596* (7873), 583−589.
(46) Michaud-Agrawal, N.; Denning, E. J.; Woolf, T. B.; Beckstein, O. MDAnalysis: a toolkit for the analysis of molecular dynamics simulations. *J. Comput. Chem.* **2011**, *32* (10), 2319−2327.
(47) Hunter, J. D. Matplotlib: A 2D Graphics Environment. *Comput. Sci. Eng.* **2007**, *9* (3), 90−95.
(48) Irwin, J. J.; Sterling, T.; Mysinger, M. M.; Bolstad, E. S.; Coleman, R. G. ZINC: A Free Tool to Discover Chemistry for Biology. *J. Chem. Inf. Model.* **2012**, *52* (7), 1757−1768.
(49) Sterling, T.; Irwin, J. J. ZINC 15 - Ligand Discovery for Everyone. *J. Chem. Inf. Model.* **2015**, *55* (11), 2324−2337.
(50) Laskowski, R. A.; Swindells, M. B. LigPlot+: Multiple Ligand-Protein Interaction Diagrams for Drug Discovery. *J. Chem. Inf. Model.* **2011**, *51*, 2778−2786.

https://doi.org/10.1021/acsomega.5c05849
ACS Omega 2025, 10, 52585−52597

3. DISCUSIÓN.

Las GTPasas esenciales Gpn1 humana y su ortólogo Npa3 en la levadura *S. cerevisiae* tienen un papel esencial en el ensamble y la acumulación nuclear de la RNA polimerasa II (Forget et al., 2010; Calera et al., 2011; Minaker et al., 2013; Niesser et al., 2016). A pesar de su importancia, se desconocen los mecanismos específicos de su funcionamiento. Npa3 en su conformación abierta exhibe una cavidad hidrofóbica que tenía unida una molécula de laurato en el cristal de Npa3, por lo que se propuso como relevante para la unión de péptidos de las subunidades de la RNA polimerasa II en experimentos bioquímicos (Niesser et al., 2016). En el presente trabajo se empleó una combinación de técnicas computacionales para evaluar las interacciones posibles de las GTPasas Npa3 y Gpn1 con péptidos de la RNAPII evaluados experimentalmente por Niesser et al., y se proponen inhibidores potenciales de su función, para su futura evaluación experimental.

La disponibilidad de la estructura cristalográfica permitió la generación del modelo de Gpn1 humana que reveló la conservación de la cavidad hidrofóbica (Figura 1 y Figura 9). El análisis de las cavidades con el software bioinformático DoGSiteScorer mostró que la cavidad que contiene el ácido graso laurato cocristalizado en la cavidad hidrofóbica propuesta como sitio de unión de péptidos, tiene el mayor volumen y potencial farmacológico tanto en el cristal de Npa3 como en el modelo de Gpn1 humana (Figura 2 y Tabla 6). Otro descriptor importante generado por DoGSite es el puntaje de potencial farmacológico, particularmente importante debido a que valores altos se asocian con una mayor probabilidad de la cavidad para unir fármacos. El valor obtenido al evaluar este parámetro en Npa3 fue considerado aceptable y como un indicador de que la cavidad hidrofóbica posee características favorables, incluyendo un volumen apropiado, accesibilidad y propiedades fisicoquímicas que la vuelven adecuada para la unión de ligandos. Por otro lado, la molécula de laurato cocristalizada en la conformación abierta de Npa3 es particularmente relevante porque actúa como un marcador de la cavidad, es decir, se une a un sitio potencialmente farmacológico en la proteína, lo que se correlaciona con los resultados de DoGSiteScorer. En este sentido y desde hace

tiempo, diversos estudios han demostrado que los ligandos cocristalizados pueden considerarse marcadores de cavidades, describiendo las propiedades fisicoquímicas, volumétricas y topológicas necesarias para el establecimiento de interacciones moleculares (Liang et al., 1998; Khazanov & Carlson, 2013; Feldmann & Bajorath, 2020). Respecto al modelado de interacciones proteína-proteína, los servidores CABS-dock y HADDOCK fueron un valioso instrumento para determinar los contactos específicos entre Npa3 y los péptidos de las subunidades Rpb1, Rpb4, Rpb8, y Rpb11. La información generada es especialmente útil debido a que no existen modelos tridimensionales disponibles para estas interacciones, la cual podría ser esencial para la biogénesis y posterior importación nuclear del complejo de la RNAPII. El acoplamiento de tipo flexible proteína-proteína y péptido proteína fue realizado a través de los servidores CABS-dock y HADDOCK 2.4 con la finalidad de evaluar la interacción de los péptidos constituyentes de la RNAPII con Npa3 mediante su cavidad hidrofóbica tanto en los péptidos individuales, como en el contexto de las subunidades completas y plegadas obtenidas desde AlphaFold2 (Figuras 3 y 10).

Los residuos más frecuentemente involucrados en las interacciones modeladas por ambos servidores fueron F143, W179, y N137 (Figura 4). En general, el número de interacciones generadas por los péptidos individuales en los modelos de CABS-dock fue aproximadamente 5.5 veces mayor que aquellos observados en HADDOCK, es decir, en el contexto de las subunidades completas. Estas diferencias se pueden atribuir a la mejor accesibilidad de Npa3 a los péptidos en los modelos de CABS-dock, en contraste con los modelos de las subunidades de la RNAPII completamente plegadas.

Particularmente para las interacciones con el péptido 21 de Rpb1, los contactos conservados se establecen entre los residuos F143 de Npa3 y A87 en Rpb1; las limitadas interacciones obtenidas fueron una consecuencia de la existencia de dos α-hélices localizadas alrededor de los péptidos definidos como activos para el acoplamiento, disminuyendo la accesibilidad por parte de Npa3. La F143 contribuye aproximadamente con una cuarta parte de todas las interacciones definidas en

consenso por CABS-dock y HADDOCK, correspondiendo a la interacción de mayor relevancia en todos los resultados de acoplamiento por HADDOCK.

El residuo F143 también está involucrado en la unión del laurato en el cristal (Figura 5). En nuestros estudios de acoplamiento sobre la estructura de Npa3, este residuo participa en la unión de los compuestos novobiocina, atovacuona, prednisolona y tibolona (Figura 6 y Tabla 2). En el caso de Gpn1, el residuo equivalente corresponder a la F166 (Figura 9), la cual participa en la interacción con ketanserina, dicumarol y atovacuona (Figura 7 y Tabla 3). Por otro lado, W179 exhibe el segundo mayor número de participaciones en las interacciones compartidas por CABS-dock y HADDOCK (Figura 4). Tanto en el cristal de Npa3, como en el modelo de Gpn1 humana, W179 establece un puente de hidrógeno con el grupo carboxilato del laurato, contribuyendo a su unión y estabilización dentro de la cavidad hidrofóbica. Respecto al acoplamiento de los fármacos aprobados por la FDA, W179 (W202 en Gpn1) estuvo involucrado en la unión de trifluperidol, novobiocina, prednisolona, y tibolona en Npa3, mediante interacciones hidrofóbicas y puentes de hidrógeno (Figuras 6 y 7). En Gpn1, el residuo equivalente W202 interactúa hidrofóbicamente con ketanserina, gliquidona, dicumarol, nefazodona, y atovacuona. De acuerdo con estos datos, los residuos F143 y W179, constituyentes de la cavidad hidrofóbica en Npa3, podrían tener un papel crítico en el reconocimiento de las subunidades de la RNA polimerasa II y en moléculas con propiedades farmacológicas. Además, se propone a estos residuos para su posterior evaluación mediante mutagénesis sitio dirigida con la finalidad se estudiar su papel en la función de Npa3.

El residuo F212 es otro residuo involucrado en la interacción de Npa3 con los ligandos evaluados y con los péptidos de la superficie de las subunidades de la RNAPII, el cual contribuye a la unión del trifluperidol y novobiocina, además, interactúa con los péptidos 201 y 234 en Rpb1 (Figuras 4 y 6). Por otro lado, F183 participa en la totalidad de las interacciones evaluadas, exceptuando al péptido 21, se une a Rpb1, Rpb4, Rpb8 y Rpb11, así como a los cinco compuestos con mayor energía de la biblioteca de la FDA.

En el presente trabajo, se utilizó al laurato cocristalizado dentro de la cavidad hidrofóbica de Npa3 como guía para validar el protocolo de acoplamiento con

AutoDock Vina. Este software fue capaz de reproducir la orientación del laurato dentro de la cavidad hidrofóbica de Npa3 abierto, indicando que es adecuado para estudiar el acoplamiento de los ligandos provenientes de la biblioteca de compuestos aprobados por la FDA, tanto en Npa3 como en el modelo de Gpn1 humano (Figura 5). Como resultado de la primera ronda de acoplamiento rígido, novobiocina se unió en la parte externa de la cavidad hidrofóbica (Figura 6B), mostrando la energía de interacción más alta junto con trifluperidol y atovacuona (Figura 6A y 6C). Novobiocina es una aminocumarina originalmente descrita como inhibidor de la DNA girasa B (Maxwell, 1993). Múltiples estudios muestran que novobiocina se une al dominio C-terminal de Hsp90, donde compite con nucleótidos y disrumpe la asociación con las cochaperonas Hsc70 y p23, provocando su inhibición. Múltiples estudios muestran que novobiocina se une al dominio C-terminal de Hsp90 (Marcu et al., 2000), donde compite con nucleótidos y desmantela la asociación de las cochaperonas p23 y Hsc70 con Hsp90, alterando su función de chaperona.

En la segunda ronda de acoplamiento, establecido de tipo flexible, se observó un incremento global en las energías de interacción para los fármacos trifluperidol, novobiocina, atovacuona, prednisolona y tibolona sobre Npa3; y de ketanserina, gliquidona, dicumarol, nefazodona, y atovacuona para el modelo de Gpn1 humano (Tabla 4 y Figura 8). Se propone que estos cambios en las energías de interacción son probablemente el resultado del ajuste inducido permitido por el acoplamiento flexible en contraste con el acoplamiento de tipo rígido.

Los resultados del acoplamiento flexible (Tabla 4) mostraron que atovacuona se une con la mejor energía en Npa3 y el homólogo humano Gpn1, sugiriendo una preferencia de unión conservada. Con la finalidad de evaluar más a profundidad la especificidad de los demás compuestos restantes, se realizó un acoplamiento cruzado o *cross-docking* (Tabla 5). El análisis mostró que todas las moléculas evaluadas muestran afinidades favorables y comparables entre ambas proteínas. Estos resultados sugieren que, además de atovacuona, los otros ligandos podrían mostrar actividad cruzada dentro de la familia GPN, lo que respalda su potencial como nuevos inhibidores del sitio de reconocimiento de la RNAPII en las GTPasas

GPN y justifica una mayor validación experimental. Por otra parte, es factible considerar que la unión de moléculas pequeñas al interior, o exterior de la cavidad hidrofóbica, puedan afectar al reconocimiento o la hidrólisis del GTP, de acuerdo con el modelo de cavidad alostérica (Stank et al., 2016), lo que sugiere la existencia de cavidades situadas en lugares distintos al catalítico con afinidad por moléculas pequeñas, donde su unión afecta a la función de la enzima. Análogamente, la unión del GTP/GDP puede verse afectada por la interacción de péptidos clave de la interfaz de las subunidades de la RNAPII con los residuos constituyentes de la cavidad hidrofóbica de Npa3 abierto. En este sentido, es esencial estudiar el posible efecto de estos péptidos sobre la actividad GTPasa de estas enzimas esenciales. Con este fin, González-González et al., publicaron en 2017 un protocolo para la purificación de la Gpn1 humana recombinante, lo que permitirá en un futuro evaluar el efecto de estos compuestos *in vitro.*

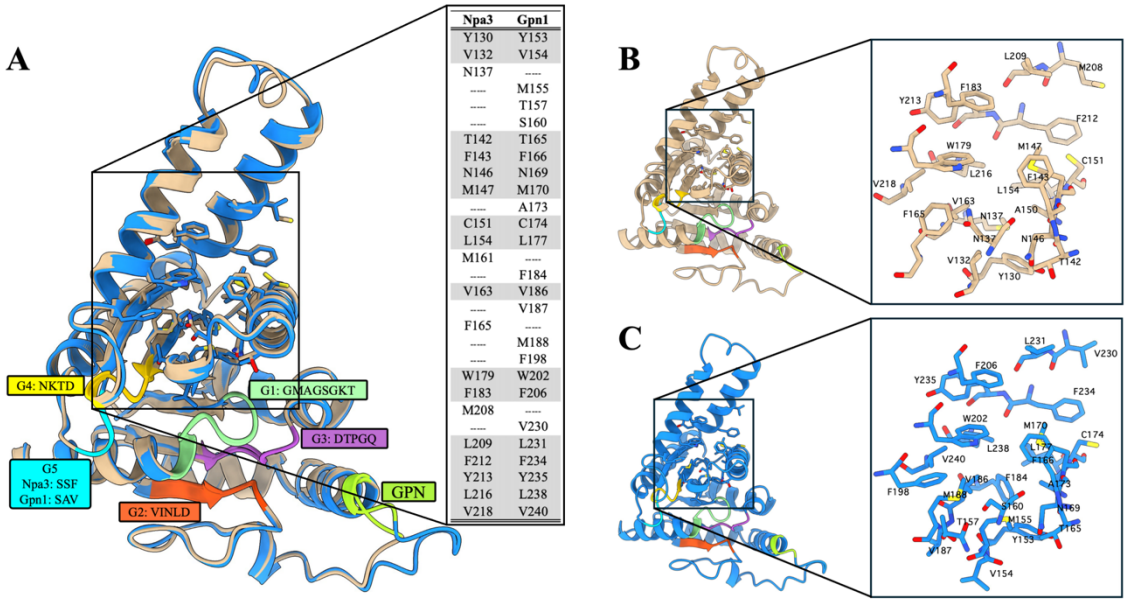

Npa3	Gpn1
Y130	Y153
V132	V154
N137	----
----	M155
----	T157
----	S160
T142	T165
F143	F166
N146	N169
M147	M170
----	A173
C151	C174
L154	L177
M161	----
----	F184
V163	V186
----	V187
F165	----
----	M188
----	F198
W179	W202
F183	F206
M208	----
----	V230
L209	L231
F212	F234
Y213	Y235
L216	L238
V218	V240

Figura 9. Orientación y equivalencias de los residuos que constituyen la cavidad hidrofóbica en Npa3 y Gpn1 abiertos. (A) Localización de los motivos GPN y G1-G5 en la representación de caricatura de Npa3 en color arena y Gpn1 en azul. En la tabla se muestra la numeración equivalente de los residuos que forman la cavidad hidrofóbica en ambas

proteínas. Los guiones en la tabla indican la ausencia de residuos equivalentes. (B) Orientación de la cadena lateral de los residuos en la cavidad hidrofóbica de Npa3 y en (C) para Gpn1.

Tabla 6. Descriptores de las propiedades globales para la forma, el tamaño y las características químicas de la cavidad de unión al laurato en Npa3 y Gpn1 en la conformación abierta.

Npa3		**Gpn1**	
Potencial farmacológico de la cavidad hidrofóbica			
0.72		0.8	
Descriptores de tamaño y forma			
Volumen (Å³)	405.89	Volumen (Å³)	482.88
Superficie (Å²)	551.69	Superficie (Å²)	640.56
Profundidad (Å)	15.47	Profundidad (Å)	16.3
Descriptores de elementos			
Número de átomos en la cavidad	100	Número de átomos en la cavidad	113
Carbonos	78	Carbonos	89
Nitrógenos	10	Nitrógenos	8
Oxígenos	10	Oxígenos	13
Azufres	2	Azufres	3
Descriptores de grupos funcionales			
Donadores de puentes de hidrógeno	6	Donadores de puentes de hidrógeno	2
Aceptores de puentes de hidrógeno	13	Aceptores de puentes de hidrógeno	17
Metales	0	Metales	0
Interacciones hidrofóbicas	38	Interacciones hidrofóbicas	50
Coeficiente de hidrofobicidad	0.67	Coeficiente de hidrofobicidad	0.72
Composición de aminoácidos			
Relación de aminoácidos apolares	0.71	Relación de aminoácidos apolares	0.72
Relación de aminoácidos polares	0.29	Relación de aminoácidos polares	0.28
Relación de aminoácidos positivos	0	Relación de aminoácidos positivos	0
Relación de aminoácidos negativos	0	Relación de aminoácidos negativos	0

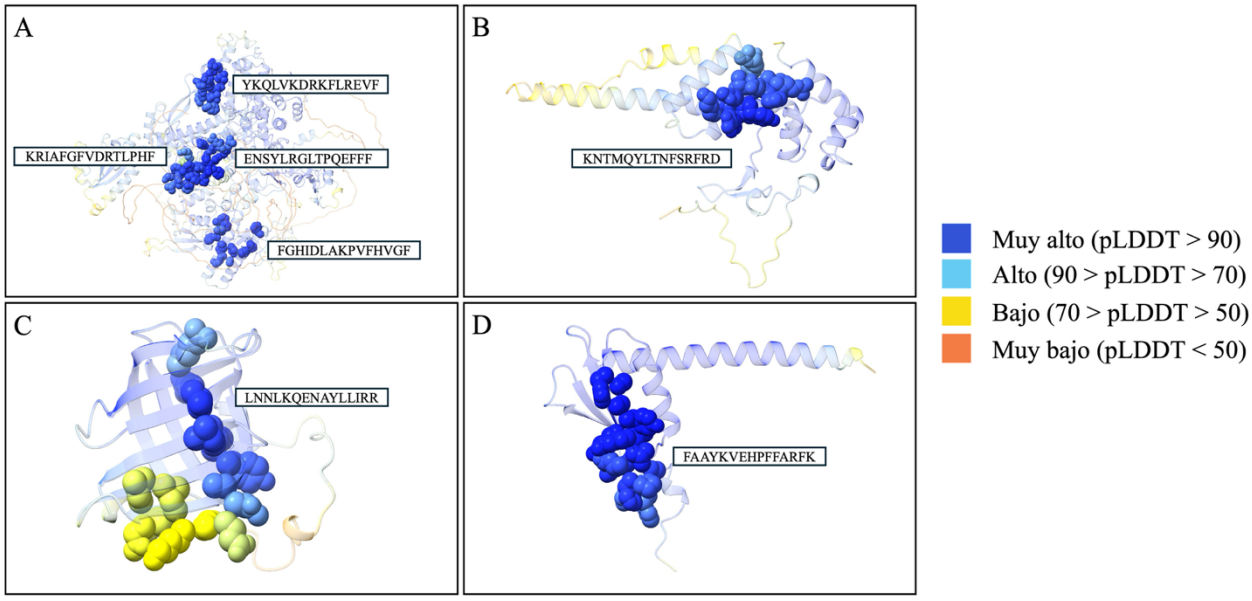

Figura 10. Intervalos de confianza para los modelos de AlphaFold2 de las subunidades (A) Rpb1, (B) Rpb4, (C) Rpb8 y (D) Rpb11 para los péptidos indicados como activos en el acoplamiento con Npa3 y Gpn1.

4. BIBLIOGRAFÍA.

1. Alonso, B., Beraud, C., Meguellati, S., Chen, S. W., Pellequer, J. L., Armengaud, J., & Godon, C. (2013). Eukaryotic GPN-loop GTPases paralogs use a dimeric assembly reminiscent of archeal GPN. *Cell Cycle*, *12*(3), 463-472. https://doi.org/10.4161/cc.23367.
2. An, J., Totrov, M., & Abagyan, R. (2004). Comprehensive identification of «druggable» protein ligand binding sites. *Genome informatics. International Conference on Genome Informatics*, *15*(2), 31-41.
3. Birnbaumer, L., Pohl, S. L., & Rodbell, M. (1971). The Glucagon-sensitive Adenyl Cyclase System in Plasma Membranes of Rat Liver. *Journal of Biological Chemistry*, *246*(6), 1857-1860. https://doi.org/10.1016/S0021-9258(18)62387-7.
4. Boulon, S., Pradet-Balade, B., Verheggen, C., Molle, D., Boireau, S., Georgieva, M., Azzag, K., Robert, M. C., Ahmad, Y., Neel, H., Lamond, A. I., & Bertrand, E. (2010). HSP90 and its R2TP/Prefoldin-like cochaperone are involved in the cytoplasmic assembly of RNA polymerase II. *Molecular Cell*, *39*(6), 912-924. https://doi.org/10.1016/j.molcel.2010.08.023.
5. Bourne, H. R., Sanders, D. A., & McCormick, F. (1990). The GTPase superfamily: A conserved switch for diverse cell functions. *Nature*, *348*(6297), 125-132. https://doi.org/10.1038/348125a0.
6. Bourne HR, DA, S., & F., M. (1991). The GTPase superfamily: Conserved structure and molecular mechanism. *Nature.*, *10*, 117-127.

7. Calera, M. R., Zamora-Ramos, C., Araiza-Villanueva, M. G., Moreno-Aguilar, C. A., Peña-Gómez, S. G., Castellanos-Terán, F., Robledo-Rivera, A. Y., & Sánchez-Olea, R. (2011). Parcs/Gpn3 is required for the nuclear accumulation of RNA polymerase II. *Biochimica et Biophysica Acta - Molecular Cell Research*, *1813*(10), 1708-1716. https://doi.org/10.1016/j.bbamcr.2011.07.005.
8. Carre, C., & Shiekhattar, R. (2011). Human GTPases Associate with RNA Polymerase II To Mediate Its Nuclear Import. *Molecular and Cellular Biology*, *31*(19), 3953-3962. https://doi.org/10.1128/MCB.05442-11.
9. Charest, P. G., & Firtel, R. A. (2007). Big roles for small GTPases in the control of directed cell movement. *Biochemical Journal*, *401*(2), 377-390. https://doi.org/10.1042/BJ20061432.
10. Chen, L., Ruan, X., Li, X., & Fu, H. (2024). Molecular Interactions in Biological Systems: Technological Applications and Innovations. *Computational Molecular Biology*. https://doi.org/10.5376/cmb.2024.14.0021.
11. De Vivo, M., Masetti, M., Bottegoni, G., & Cavalli, A. (2016). Role of Molecular Dynamics and Related Methods in Drug Discovery. *Journal of Medicinal Chemistry*, *59*(9), 4035-4061. https://doi.org/10.1021/acs.jmedchem.5b01684.
12. Der, C. J., Krontiris, T. G., & Cooper, G. M. (1982). Transforming genes of human bladder and lung carcinoma cell lines are homologous to the ras genes of Harvey and Kirsten sarcoma viruses. *Proceedings of the National Academy of Sciences*, *79*(11), 3637-3640. https://doi.org/10.1073/pnas.79.11.3637.

13. Erickson, J. A., Jalaie, M., Robertson, D. H., Lewis, R. A., & Vieth, M. (2004). Lessons in Molecular Recognition: The Effects of Ligand and Protein Flexibility on Molecular Docking Accuracy. *Journal of Medicinal Chemistry*, *47*(1), 45-55. https://doi.org/10.1021/jm030209y.
14. Feldmann, C., & Bajorath, J. (2020). X-ray Structure-Based Chemoinformatic Analysis Identifies Promiscuous Ligands Binding to Proteins from Different Classes with Varying Shapes. *International Journal of Molecular Sciences*, *21*(11), 3782. https://doi.org/10.3390/ijms21113782.
15. Ferreira, L., Dos Santos, R., Oliva, G., & Andricopulo, A. (2015). Molecular Docking and Structure-Based Drug Design Strategies. *Molecules*, *20*(7), 13384-13421. https://doi.org/10.3390/molecules200713384.
16. Fink, F., Ederer, S., & Gronwald, W. (2009). Protein-Protein Interaction Analysis by Docking. *Algorithms*, *2*(1), 429-436. https://doi.org/10.3390/a2010429.
17. Forget, D., Lacombe, A.-A., Cloutier, P., Al-Khoury, R., Bouchard, A., Lavallée-Adam, M., Faubert, D., Jeronimo, C., Blanchette, M., & Coulombe, B. (2010). The Protein Interaction Network of the Human Transcription Machinery Reveals a Role for the Conserved GTPase RPAP4/GPN1 and Microtubule Assembly in Nuclear Import and Biogenesis of RNA Polymerase II. *Molecular & Cellular Proteomics*, *9*(12), 2827-2839. https://doi.org/10.1074/mcp.M110.003616.
18. Frasnetti, E., Magni, A., Castelli, M., Serapian, S. A., Moroni, E., & Colombo, G. (2024). Structures, dynamics, complexes, and functions: From classic

computation to artificial intelligence. *Current Opinion in Structural Biology*, *87*, 102835. https://doi.org/10.1016/j.sbi.2024.102835.

19. González-González, R., Guerra-Moreno, J. A., Cristóbal-Mondragón, G. R., Romero, V., Peña-Gómez, S. G., Montero-Morán, G. M., Lara-González, S., Hernández-Arana, A., Fernández-Velasco, D. A., Calera, M. R., & Sánchez-Olea, R. (2017). Human Gpn1 purified from bacteria binds guanine nucleotides and hydrolyzes GTP as a protein dimer stabilized by its C-terminal tail. *Protein Expression and Purification*, *132*, 85-96. https://doi.org/10.1016/j.pep.2017.01.009.
20. Goodsell, D. S., & Olson, A. J. (1990). Automated docking of substrates to proteins by simulated annealing. *Proteins: Structure, Function, and Bioinformatics*, *8*(3), 195-202. https://doi.org/10.1002/prot.340080302.
21. Goodsell, D. S., & Olson, A. J. (2000). Structural Symmetry and Protein Function. *Annual Review of Biophysics and Biomolecular Structure*, *29*(1), 105-153. https://doi.org/10.1146/annurev.biophys.29.1.105.
22. Gordon, J. (1969). Hydrolysis of Guanosine 5'-Triphosphate Associated with Binding of Aminoacyl Transfer Ribonucleic Acid to Ribosomes. *Journal of Biological Chemistry*, *244*(20), 5680-5686. https://doi.org/10.1016/S0021-9258(18)63613-0.
23. Gras, S., Chaumont, V., Fernandez, B., Carpentier, P., Charrier-Savournin, F., Schmitt, S., Pineau, C., Flament, D., Hecker, A., Forterre, P., Armengaud, J., & Housset, D. (2007). Structural insights into a new homodimeric self-activated GTPase family. *EMBO Reports*, *8*(6), 569-575. https://doi.org/10.1038/sj.embor.7400958.

24. Grassmann, G., Miotto, M., Desantis, F., Di Rienzo, L., Tartaglia, G. G., Pastore, A., Ruocco, G., Monti, M., & Milanetti, E. (2024). Computational Approaches to Predict Protein–Protein Interactions in Crowded Cellular Environments. *Chemical Reviews*, *124*(7), 3932-3977. https://doi.org/10.1021/acs.chemrev.3c00550.
25. Hall, A. (1990). The Cellular Functions of Small GTP-Binding Proteins. *Science, New Series*, *249*(4969), 635-640.
26. Harmalkar, A., & Gray, J. J. (2021). Advances to tackle backbone flexibility in protein docking. *Current Opinion in Structural Biology*, *67*, 178-186. https://doi.org/10.1016/j.sbi.2020.11.011.
27. Hughes, J., Rees, S., Kalindjian, S., & Philpott, K. (2011). Principles of early drug discovery. *British Journal of Pharmacology*, *162*(6), 1239-1249. https://doi.org/10.1111/j.1476-5381.2010.01127.x.
28. Khazanov, N. A., & Carlson, H. A. (2013). Exploring the Composition of Protein-Ligand Binding Sites on a Large Scale. *PLoS Computational Biology*, *9*(11), e1003321. https://doi.org/10.1371/journal.pcbi.1003321.
29. Kitchen, D. B., Decornez, H., Furr, J. R., & Bajorath, J. (2004). Docking and scoring in virtual screening for drug discovery: Methods and applications. *Nature Reviews Drug Discovery*, *3*(11), 935-949. https://doi.org/10.1038/nrd1549.
30. Kuntz, I. D., Blaney, J. M., Oatley, S. J., Langridge, R., & Ferrin, T. E. (1982). *A Geometric Approach to Macromolecule-Ligand Interactions*.

31. Lee, J., Hao Nguyen, C., & Mamitsuka, H. (2025). Beyond rigid docking: Deep learning approaches for fully flexible protein–ligand interactions. *Briefings in Bioinformatics*, *26*(5), bbaf454. https://doi.org/10.1093/bib/bbaf454.
32. Leipe, D. D., Wolf, Y. I., Koonin, E. V., & Aravind, L. (2002). Classification and evolution of P-loop GTPases and related ATPases. *Journal of Molecular Biology*, *317*(1), 41-72. https://doi.org/10.1006/jmbi.2001.5378.
33. Lengauer, T., & Rarey, M. (1996). Computational methods for biomolecular docking. *Current Opinion in Structural Biology*, *6*(3), 402-406. https://doi.org/10.1016/S0959-440X(96)80061-3.
34. Li, M. (2024). Molecular Dynamics Simulations: A Systematic Review of Techniques and Applications in Biochemistry. *Computational Molecular Biology*. https://doi.org/10.5376/cmb.2024.14.0029.
35. Liang, J., Woodward, C., & Edelsbrunner, H. (1998). Anatomy of protein pockets and cavities: Measurement of binding site geometry and implications for ligand design. *Protein Science*, *7*(9), 1884-1897. https://doi.org/10.1002/pro.5560070905.
36. Londos, C., Salomon, Y., Lin, M. C., Harwood, J. P., Schramm, M., Wolff, J., & Rodbell, M. (1974). 5′-Guanylylimidodiphosphate, A Potent Activator of Adenylate Cyclase Systems in Eukaryotic Cells. *Proceedings of the National Academy of Sciences*, *71*(8), 3087-3090. https://doi.org/10.1073/pnas.71.8.3087.
37. Marcu, M. G., Chadli, A., Bouhouche, I., Catelli, M., & Neckers, L. M. (2000). The heat shock protein 90 antagonist novobiocin interacts with a previously unrecognized ATP-binding domain in the carboxyl terminus of the chaperone.

Journal of Biological Chemistry, *275*(47), 37181-37186. https://doi.org/10.1074/jbc.M003701200.

38. Matte-Tailliez, O., Zivanovic, Y., & Forterre, P. (2000). Mining archaeal proteomes for eukaryotic proteins with novel functions: *Trends in Genetics*, *16*(12), 533-536. https://doi.org/10.1016/S0168-9525(00)02137-5.
39. Maxwell, A. (1993). The interaction between coumarin drugs and DNA gyrase. *Molecular Microbiology*, *9*(4), 681-686. https://doi.org/10.1111/j.1365-2958.1993.tb01728.x.
40. Meng, X.-Y., Zhang, H.-X., Mezei, M., & Cui, M. (2011). Molecular Docking: A Powerful Approach for Structure-Based Drug Discovery. *Current Computer Aided-Drug Design*, *7*(2), 146-157. https://doi.org/10.2174/157340911795677602.
41. Milburn, M. V., Tong, L., deVos, A. M., Brünger, A., Yamaizumi, Z., Nishimura, S., & Kim, S.-H. (1990). Molecular Switch for Signal Transduction: Structural Differences between Active and Inactive Forms of Protooncogenic ras Proteins. *Science, New Series*, *247*(4945), 939-945.
42. Minaker, S. W., Filiatrault, M. C., Ben-Aroya, S., Hieter, P., & Stirling, P. C. (2013). Biogenesis of RNA polymerases II and III requires the conserved GPN small GTPases in Saccharomyces cerevisiae. *Genetics*, *193*(3), 853-864. https://doi.org/10.1534/genetics.112.148726.
43. Miyazono, K., & Tanokura, M. (2022). New era in structural biology with the AlphaFold program. *Translational and Regulatory Sciences*, *4*(2), 48-52. https://doi.org/10.33611/trs.2022-005.

44. Mondal, A., Chang, L., & Perez, A. (2022). Modelling peptide–protein complexes: Docking, simulations and machine learning. *QRB Discovery*, *3*, e17. https://doi.org/10.1017/qrd.2022.14.

45. Niesser, J., Wagner, F. R., Kostrewa, D., Mühlbacher, W., & Cramer, P. (2016). Structure of GPN-Loop GTPase Npa3 and Implications for RNA Polymerase II Assembly. *Molecular and Cellular Biology*, *36*(5), 820-831. https://doi.org/10.1128/mcb.01009-15.

46. Nussinov, R., Tsai, C.-J., Shehu, A., & Jang, H. (2019). Computational Structural Biology: Successes, Future Directions, and Challenges. *Molecules*, *24*(3), 637. https://doi.org/10.3390/molecules24030637.

47. Paduch, M., Jeleń, F., & Otlewski, J. (2001). Structure of small G proteins and their regulators. *Acta Biochimica Polonica*, *48*(4), 829-850. https://doi.org/10.18388/abp.2001_3850.

48. Pagadala, N. S., Syed, K., & Tuszynski, J. (2017). Software for molecular docking: A review. *Biophysical Reviews*, *9*(2), 91-102. https://doi.org/10.1007/s12551-016-0247-1.

49. Pai, E. F., Kabsch, W., Krengel, U., Holmes, K. C., John, J., & Wittinghofer, A. (1989). Structure of the guanine-nucleotide-binding domain of the Ha-ras oncogene product p21 in the triphosphate conformation. *Nature*, *341*(6239), 209-214. https://doi.org/10.1038/341209a0.

50. Pérot, S., Sperandio, O., Miteva, M. A., Camproux, A.-C., & Villoutreix, B. O. (2010). Druggable pockets and binding site centric chemical space: A paradigm shift in drug discovery. *Drug Discovery Today*, *15*(15-16), 656-667. https://doi.org/10.1016/j.drudis.2010.05.015.

51. Reiner, D. J. (2018). Small GTPases. *WormBook*, 1-65. https://doi.org/10.1895/wormbook.1.67.2.

52. Rodbell, M., Birnbaumer, L., Pohl, S. L., & Krans, H. M. J. (1971). The Glucagon-sensitive Adenyl Cyclase System in Plasma Membranes of Rat Liver. *Journal of Biological Chemistry*, *246*(6), 1877-1882. https://doi.org/10.1016/S0021-9258(18)62390-7.

53. Rojas, A. M., Fuentes, G., Rausell, A., & Valencia, A. (2012). The Ras protein superfamily: Evolutionary tree and role of conserved amino acids. *Journal of Cell Biology*, *196*(2), 189-201. https://doi.org/10.1083/jcb.201103008.

54. Ru, X., Zhao, S., Zou, Q., & Xu, L. (2024). Identify potential drug candidates within a high-quality compound search space. *Briefings in Bioinformatics*, *26*(1), bbaf024. https://doi.org/10.1093/bib/bbaf024.

55. Santos, E., Tronick, S. R., Aaronson, S. A., Pulciani, S., & Barbacid, M. (1982). T24 human bladder carcinoma oncogene is an activated form of the normal human homologue of BALB- and Harvey-MSV transforming genes. *Nature*, *298*(5872), 343-347. https://doi.org/10.1038/298343a0.

56. Son, A., Kim, W., Park, J., Lee, W., Lee, Y., Choi, S., & Kim, H. (2024). Utilizing Molecular Dynamics Simulations, Machine Learning, Cryo-EM, and NMR Spectroscopy to Predict and Validate Protein Dynamics. *International Journal of Molecular Sciences*, *25*(17), 9725. https://doi.org/10.3390/ijms25179725

57. Sprang, S. R. (1997). G PROTEIN MECHANISMS: Insights from Structural Analysis. *Annual Review of Biochemistry*, *66*(1), 639-678. https://doi.org/10.1146/annurev.biochem.66.1.639.

58. Stank, A., Kokh, D. B., Fuller, J. C., & Wade, R. C. (2016). Protein Binding Pocket Dynamics. *Accounts of Chemical Research*, *49*(5), 809-815. https://doi.org/10.1021/acs.accounts.5b00516.

59. Staresincic, L., Walker, J., Dirac-Svejstrup, A. B., Mitter, R., & Svejstrup, J. Q. (2011). GTP-dependent binding and nuclear transport of RNA polymerase II by Npa3 protein. *Journal of Biological Chemistry*, *286*(41), 35553-35561. https://doi.org/10.1074/jbc.M111.286161.

60. Takai, Y., Sasaki, T., & Matozaki, T. (2001). Small GTP-Binding Proteins. *American Physiological Society*, *81*(1), 153-208. https://doi.org/10.1152/physrev.2001.81.1.153.

61. Valencia, A., Chardin, P., Wittinghofer, A., & Sander, C. (1991). The ras protein family: Evolutionary tree and role of conserved amino acids. *Biochemistry*, *30*(19), 4637-4648. https://doi.org/10.1021/bi00233a001.

62. Vetter, I. R., & Wittinghofer, A. (2001). The Guanine Nucleotide-Binding Switch in Three Dimensions. *Science, New Series*, *294*(5545), 1299-1304.

63. Walker, J. E., Saraste, M., Runswick, M. J., & Gay, N. J. (1982). Distantly related sequences in the alpha- and beta-subunits of ATP synthase, myosin, kinases and other ATP-requiring enzymes and a common nucleotide binding fold. *The EMBO Journal*, *1*(8), 945-951. https://doi.org/10.1002/j.1460-2075.1982.tb01276.x.

64. Walters, W. P., & Murcko, M. A. (2002). Prediction of ‘drug-likeness’. *Advanced Drug Delivery Reviews*, *54*(3), 255-271. https://doi.org/10.1016/S0169-409X(02)00003-0.

65. Wennerberg, K., Rossman, K. L., & Der, C. J. (2005). The Ras superfamily at a glance. *Journal of Cell Science*, *118*(5), 843-846. https://doi.org/10.1242/jcs.01660.

66. Wild, T., & Cramer, P. (2012). Biogenesis of multisubunit RNA polymerases. *Trends in Biochemical Sciences*, *37*(3), 99-105. https://doi.org/10.1016/j.tibs.2011.12.001.

67. Yalovsky, S., Bloch, D., Sorek, N., & Kost, B. (2008). Regulation of Membrane Trafficking, Cytoskeleton Dynamics, and Cell Polarity by ROP/RAC GTPases. *Plant Physiology*, *147*(4), 1527-1543. https://doi.org/10.1104/pp.108.122150

68. Zhang, J., & Qian, J. (2024). Advances in Computational Intelligence-Based Methods of Structure and Function Prediction of Proteins. *Biomolecules*, *14*(9), 1083. https://doi.org/10.3390/biom14091083.

69. Zhu, H., Zhang, Y., Li, W., & Huang, N. (2022). A Comprehensive Survey of Prospective Structure-Based Virtual Screening for Early Drug Discovery in the Past Fifteen Years. *International Journal of Molecular Sciences*, *23*(24), 15961. https://doi.org/10.3390/ijms232415961.